LAWRENCE
LIVERMORE
NATIONAL
LABORATORY

LLNL-TR-676592

Generalized Lawson Criteria for Inertial Confinement Fusion

R. E. Tipton

August 27, 2015

Disclaimer

This work performed under the auspices of the U.S. Department of Energy by Lawrence Livermore National Laboratory under Contract DE-AC52-07NA27344.

Generalized Lawson Criteria for Inertial Confinement Fusion

Robert Tipton

January 15, 2015

The Lawson Criterion was proposed by John D. Lawson in 1955 as a general measure of the conditions necessary for a magnetic fusion device to reach thermonuclear ignition. Over the years, similar ignition criteria have been proposed which would be suitable for Inertial Confinement Fusion (ICF) designs. This paper will compare and contrast several ICF ignition criteria based on Lawson's original ideas. Both analytical and numerical results will be presented which will demonstrate that although the various criteria differ in some details, they are closely related and perform similarly as ignition criteria. A simple approximation will also be presented which allows the inference of each ignition parameter directly from the measured data taken on most shots fired at the National Ignition Facility (NIF) with a minimum reliance on computer simulations. Evidence will be presented which indicates that the experimentally inferred ignition parameters on the best NIF shots are very close to the ignition threshold.

I. Introduction

In 1955 John D. Lawson proposed two different ignition criteria for the deuterium-tritium (DT) plasma in a magnetic fusion device [Lawson 1955]. The more famous was $n\tau > 1.5x10^{14}$ *sec/cc* – where n is the DT plasma density in atoms/cc and τ is the plasma confinement time in seconds. The less famous but more useful criterion was the triple product: $nT\tau > 3x10^{15}$ *KeV-sec/cc* – where T is the temperature of the DT plasma in KeV. The triple product can easily be expressed as pressure times τ or $P\tau >$ 9.6 atm-sec. The exact threshold values for both criteria are dependent on the temperature of the plasma.

While the Lawson criteria were originally designed for magnetically confined fusion plasmas, many people saw the value of generalizing Lawson's original criteria to the context of Inertial Confinement Fusion (ICF). One such example is the work of Ricardo Betti who published a $P\tau$ or χ criterion in 2010 [Betti 2010] which is essentially the same as Lawson's Triple Product $nT\tau$.

Several other ignition criteria have been proposed [Cheng 2014] including a family of ignition criteria in the form of:

$$\rho RT^n > Threshold \tag{1.1}$$

We will also examine a modification of an ignition parameter introduced by Jim Slone and Mike Larson of LLNL.

$$\eta = \frac{Y_{no-\alpha}}{E_{max}} \tag{1.2}$$

$Y_{no\text{-}\alpha}$ is the yield of the hotspot with the alpha energy depositions turned off. E_{max} is the maximum of the hotspot thermal energy.

Another important ignition criterion is the Ignition Threshold Factor Experimental or ITFX developed at the Lawrence Livermore National Laboratory (LLNL):

$$ITFX = \left(\frac{Y_n}{3.2\times10^{15}}\right)\left(\frac{DSR}{0.07}\right)^{2.3} > 1.0 \tag{1.3}$$

Yn is the measured neutron yield of the shot and DSR is measured Down Scattered Ratio which is the number of measured neutrons between 10 and 12 MeV divided by the number of measured neutrons between 13 and 15 MeV.

In this paper it will be shown the ρRT^n ignition criterion of equation 1.1 is closely related to the more familiar $P\tau$ version of the Lawson Criterion. We will also show that the Slone-Larson ignition parameter defined in equation 1.2 is equivalent to Betti's χ and both can be derived from Lawson's fundamental hypothesis. It has been shown elsewhere [Betti 2010, Lindl 2014] that a simple generalization of the χ criterion is closely related to ITFX. Hence we are led to the conclusion that most if not all ICF criteria in use today are variations of Lawson's original idea.

Section II will develop Lawson's original hypothesis and show how it is related to Betti's χ, ρRT^2 and the Slone-Larson η. Section III will present the bare DT sphere problem originally due to Heiner Meldner and generalize it to include the physics of inertial tamping due to the cold fuel ice. Section IV will show how all of the ignition parameters discussed in this paper can be extracted from actual NIF data with minimal reliance on code simulations. Section V will present the results of 500 drive variations of a typical NIF design and show how well each of the ignition parameters perform as ignition criteria. Section VI will present the ignition parameters measured on actual NIF shots and compare them with the behavior of code simulations. This comparison will demonstrate that the best NIF shots are close to the expected ignition threshold. Finally section VII will finish up with some conclusions.

II. Lawson's Criterion with Generalizations

Lawson's principal assumption was that ignition will occur whenever the heating rate due to thermonuclear reactions exceeds the plasma cooling rate due to various loss mechanisms:

$$\dot{E}_{TN} > \frac{E_{Plasma}}{\tau} \tag{2.1}$$

E_{Plasma} is the thermal energy of the ions and the electrons. $\dot{E}_{TN}$ is the thermonuclear energy deposition rate in the plasma. It has units of energy per time per volume. Finally τ is the plasma confinement time or energy dissipation time.

The thermonuclear energy deposition rate per volume of the plasma is:

$$\dot{E}_{TN} = n^2 \chi_D \chi_T \langle \sigma v(T) \rangle K_B T_\alpha \tag{2.2}$$

The symbol n is the ion number density. χ_D and χ_T are the deuterium and tritium atom fractions which are normally set to 0.5 for an equimolar mixture. $K_B = 1.60217657 \times 10^{-9}$ is the Boltzmann constant which converts temperature from Kilovolts into energy in ergs. T_α = 3541 KeV is the energy of the D+T alpha particle in Kilovolts. $<\sigma v(T)>$ is the Maxwell averaged thermonuclear reaction rate for the D+T reaction at temperature T. $<\sigma v>$ conventionally has units of cm^3/sec.

Equation 2.2 assumes all of the energy of the 3.5 MeV alpha particles is instantly deposited into the DT plasma and that all of the 14.1 MeV thermonuclear neutrons escape the plasma without depositing any energy.

The energy of the plasma is given by the ideal gas law:

$$E_{Plasma} = 2\left(\frac{3}{2} n K_B T\right) \tag{2.3}$$

The factor or 2 comes from the fact that for plasmas consisting of hydrogen isotopes, the ions and electrons contribute equally to the thermal energy. Equation 2.3 assumes that the plasma is fully ionized and the electrons and ions are in thermal equilibrium and characterized by a single plasma temperature T. The heat capacity of the radiation field has been ignored.

Putting equations 2.2 and 2.3 into 2.1 leads to:

$$nT\tau > \frac{12}{T_\alpha} \frac{T^2}{\langle \sigma v \rangle} \left[\frac{1}{4 \chi_D \chi_T}\right] \tag{2.4}$$

The function $T^2/\langle\sigma v\rangle$ has a minimum at 13.6 KeV and at this temperature if we put in the numbers for a equimolar mixture of DT we get:

$$nT\tau > 3.0 \times 10^{15} \tag{2.5}$$

This is the usual form of Lawson's triple product, but it is easy to re-express the triple product in terms of Pτ. The material pressure of a fully ionized plasma is:

$$P = 2K_B nT \tag{2.6}$$

Again the factor of two comes from the fact that both the ions and electrons contribute equally to the pressure. Combining equations 2.4 and 2.6 together gives an expression for Pτ:

$$P\tau > \frac{24K_B}{T_\alpha}\left(\frac{T^2}{\langle\sigma v\rangle}\right)\left[\frac{1}{4\chi_D\chi_T}\right] \tag{2.7}$$

Equation 2.7 shows that the exact value of the Pτ threshold for ignition depends on the plasma temperature. For this reason, by itself, Pτ is not a very good ignition parameter. This problem can be addressed by introducing the Pτ ignition threshold function as:

$$(P\tau)_{ig} = \frac{24K_B}{T_\alpha}\left(\frac{T^2}{\langle\sigma v\rangle}\right)\left[\frac{1}{4\chi_D\chi_T}\right] \tag{2.8a}$$

$$(P\tau)_{ig} = 1.086 \times 10^{-17}\left(\frac{T^2}{\langle\sigma v\rangle}\right)\left[\frac{1}{4\chi_D\chi_T}\right] \tag{2.8b}$$

$(P\tau)_{ig}$ in the second equation 2.8b will be in units of Gb-ns if the temperature is in KeV and $\langle\sigma v\rangle$ has units of cm^3/sec. Note that gigibars-nanoseconds (Gb-ns) is equivalent to atmosphere-seconds.

Over a limited range of temperatures, the Maxwell averaged D+T reaction can be approximated as a power law:

$$\langle\sigma v\rangle = \langle\sigma v\rangle_0 T^b \tag{2.9a}$$

For 3.0 KeV < T < 4.2 KeV $b = 4.01$ and $\langle\sigma v\rangle_0 = 2.2160 \times 10^{-20}$ cc/sec (2.9b)

For 4.0 KeV < T < 6.0 KeV $b = 3.59$ and $\langle\sigma v\rangle_0 = 4.0113 \times 10^{-20}$ cc/sec (2.9c)

Putting equation 2.8b into 2.9b gives a power law expression for $(P\tau)_{ig}$:

$$(P\tau)_{ig} = 490.0\left(\frac{1}{T^{2.01}}\right)\left[\frac{1}{4\chi_D\chi_T}\right] \tag{2.10}$$

Again T is in KeV and $(P\tau)_{ig}$ is in Gb-ns or atm-sec.

Ricardo Betti introduced a new ignition parameter he labeled χ [Betti 2010], which is defined as:

$$\chi = \frac{P\tau}{(P\tau)_{ig}} = 9.21 \times 10^{16} P\tau \frac{\langle\sigma v\rangle}{T^2}[4\chi_D\chi_T] \quad (2.11a)$$

$$\chi = 2.041 \times 10^{-3} P\tau T^{2.01}[4\chi_D\chi_T] \quad (2.11b)$$

The ignition condition is simply that χ must exceed unity.

In his 2010 paper Betti goes on to make a number of analytic approximations for χ which allow him to compare χ to ITFX. However in most applications, it is simpler and perhaps more accurate to leave χ defined in terms of P, τ and T. These values can be taken from either code simulations or inferred directly from experiment.

The usual practice is to calculate ignition parameters like χ using simulations in which the energy deposition due to the 3.5 MeV thermonuclear alpha particle is ignored. These are known as no-alpha calculations. This is done because the ignition threshold appears very sharp when the calculated capsule yield with alpha depositions on is plotted against χ with alpha depositions off. But one must keep in mind that this is an artificial trick. In nature, it not possible to shut off alpha depositions and for this reason the values of χ inferred from actually NIF shots should be compared to calculations with alpha depositions turned on.

There is a way to experimental measure the no-alpha value of χ on some NIF shots. The trick is to use DT ice in which the deuterium concentration is kept very low and hydrogen is introduced. If the concentrations of tritium and hydrogen are adjusted properly the initial density of the DT and the ionized equation of state can be made very close to the case of an equimolar mix of deuterium and tritium. However because the concentration of deuterium is low, alpha depositions from the D+T reaction will never become significant enough to deviate from the no-alpha case.

The Slone-Larson Figure-of-Merit

In the 1970's and 1980's, Jim Slone and Mike Larson of Livermore defined their own ignition parameter which unknown to them was a slight variation of Lawson's criterion. Slone's original figure-of-merit was simply the specific yield of a no-alpha calculation:

$$FOM_{Slone} = \frac{Y_{no-\alpha}}{M_{DT}} \quad (2.12)$$

The definition of $Y_{no-\alpha}$ is a little confusing. It is the total of all the alpha energy produced in a calculation in which the alpha particles are produced but not allowed to deposit any energy back into the hotspot. M_{DT} is the mass of the DT in the hotspot [Slone 1983].

Mike Larson argued that the FOM needed to take into account the temperature of the hotspot. Larson reasoned that the hotter a hotspot was, the more rapidly heat conduction would cool it. Larson's figure-of-merit was:

$$FOM_{Larson} = \frac{Y_{no-\alpha}}{M_{DT}(T^*)^{5/2}} \tag{2.13}$$

The exponent of 5/2 was chosen because the Spitzer thermal conductivity is proportional to the plasma temperature raised to the 5/2 power. The characteristic temperature T* (also known as the breakaway temperature) was defined as the spatially averaged hotspot temperature with alpha depositions off at the point in time when the average hotspot temperature with alpha depositions on exceeded the hotspot temperature with alpha depositions off by exactly 5%. This sounds confusing but in simple terms T* is the temperature at which the alpha-on and alpha-off calculations first begin to diverge from one another [Larson 1983].

I worked with both Jim Slone and Mike Larson closely during the 1980's and I never heard either of them mention any idea that their figures-of-merit were is some way related to the Lawson criterion. At the time it didn't occur to me that their criteria was related to Lawson's and very likely it never occurred to either of them.

However today it is obvious that Slone and Larson were very close to a variation of the Lawson criterion. If instead of the break-away temperature to the 5/2 power, Larson had used the maximum no-alpha hotspot temperature to the first power, he would have come very close to something proportional to Betti's χ.

$$FOM_{Larson-modifed} = \frac{Y_{no-\alpha}}{M_{DT}T_{max}} \tag{2.14}$$

To see this let's go back to Lawson's starting hypothesis in equations 2.1:

$$\dot{E}_{TN} > \frac{E_{Plasma}}{\tau} \tag{2.1}$$

Both the thermonuclear energy deposition rate and the plasma energy in equation 2.1 are expressed as energy per cubic volume. However there is no reason equation 2.1 cannot be integrated over the entire hotspot volume to give:

$$\dot{Y}_{\alpha} > \frac{E_{Total\ Hotspot}}{\tau} \tag{2.15}$$

$\dot{Y}_\alpha$ is the total instantaneous thermonuclear alpha energy production rate integrated over the entire hotspot and $E_{Total\ Hotspot}$ is the thermal energy of the hotspot. Equation 2.15 can be rearranged slightly to give:

$$\eta = \frac{\dot{Y}_\alpha \tau}{E_{Total\ Hotspot}} > 1 \tag{2.16}$$

It may not be obvious, but the dimensionless ratio defined as η in equation 2.16 is essentially the same as Betti's χ in equation 2.11. Only one step is left to transform equation 2.16 into the modified Larson figure of merit and that is to replace $\dot{Y}_\alpha \tau$ by the time integrated yield of the hotspot.

$$\eta = \frac{Y_{no-\alpha}}{E_{Max\ no-\alpha}} > 1 \tag{2.17a}$$

With

$$Y_{no-\alpha} = \int \dot{Y}_\alpha dt \tag{2.17b}$$

The definition of $Y_{no-\alpha}$ here in equation 2.17 is the same as the no-alpha yield used by Slone and Larson. The definition of $E_{Max\ no-\alpha}$ is the maximum thermal energy of the hotspot in a no-alpha calculation. Notice that $E_{Max\ no-\alpha}$ should be proportional to $M_{DT}T_{max}$. This completes the proof that the modified version of the Slone-Larson figure-of-merit in equation 2.14 is a variation of the Lawson criterion and is in fact proportional to Betti's χ.

The ρRT^n Ignition Criteria

It is easy to convert the Lawson criterion or Betti's χ criterion into an ignition criterion involving ρRT^n [Cheng 2014]. The exact value of the temperature exponent *n* depends on the power law used to approximate the thermonuclear reaction rate $<\sigma v>$. However numerical simulation in section III indicate that generally n = 2 gives the best overall results.

We begin with Lawson's expression for the triple product found in equation in 2.4:

$$nT\tau > \frac{12}{T_\alpha}\frac{T^2}{\langle \sigma v \rangle}\left[\frac{1}{4\chi_D\chi_T}\right] \tag{2.4}$$

Note that the ion number density is proportional to the mass density:

$$n = \frac{N_0 \rho}{\bar{A}} \tag{2.18}$$

$N_0 = 6.0221413 \times 10^{23}$ is Avogadro's number. $\bar{A}$ is the atomic mass of the DT plasma and ρ is the mass density. The atomic mass depends slightly on the composition of the DT plasma:

$$\bar{A} = A_D\chi_D + A_T\chi_T = A_{DT}\left(\frac{A_D}{A_{DT}}\chi_D + \frac{A_T}{A_{DT}}\chi_T\right) = A_{DT}(0.8\chi_D + 1.2\chi_T) \tag{2.19}$$

A_D = 2.014102 is the deuteron mass. A_T = 3.016050 is the triton mass and A_{DT} = 2.5373 is the average atomic mass of an equimolar DT mixture. Putting equations 2.18 and 2.19 into equation 2.4 and rearranging a little gives:

$$\rho T^2\tau > \frac{12A_{DT}}{N_0 T_\alpha}\frac{T^3}{\langle\sigma v\rangle}\left[\frac{0.8\chi_D+1.2\chi_T}{4\chi_D\chi_T}\right] \tag{2.20}$$

Now it is necessary to make an approximation for the time scale τ. The obvious choice is to set τ equal to the sonic transit time across both the hotspot and the cold fuel:

$$\tau = \frac{R}{C_h} + \frac{\Delta R}{C_c} = \frac{R}{C_h}\left(1 + \frac{\Delta R C_h}{R C_c}\right) \tag{2.21}$$

R is the radius of the hotspot and ΔR is the radial thickness of the DT ice shell surrounding the hotspot. C_h is the speed of sound of the hotspot and C_c is the speed of sound of the cold fuel. The hotspot is not degenerate and therefore the ideal gas is a good approximation. The speed of sound for an ideal gas can be expressed as:

$$C_h = \sqrt{\frac{\gamma P}{\rho}} \tag{2.22}$$

P is the pressure of the hotspot and ρ is the density of the hotspot. γ is the adiabatic exponent for an ideal gas which is 5/3.

The cold fuel is degenerate and the ideal gas law is not an appropriate. Instead we may approximate the electrons of the cold fuel as a degenerate Thomas-Fermi gas in which case the pressure is:

$$P_c = b\rho_c^{5/3} \tag{2.23}$$

P_c is the pressure of the cold fuel and ρ_c is the density of the cold fuel. The symbol *b* is a constant. The speed of sound squared for a Thomas-Fermi gas is:

$$C_c^2 = \frac{\partial P_c}{\partial \rho} = \frac{5}{3}\frac{P_c}{\rho_c} \tag{2.24}$$

Nature is very kind to us here. Even though the cold fuel cannot be described by the ideal gas, the speed of sound for the cold fuel takes on the same form as the speed of sound for an ideal gas.

$$C_c = \sqrt{\frac{\gamma P_c}{\rho_c}} \tag{2.25}$$

Even the adiabatic gamma for the Thomas-Fermi gas is the same as the adiabatic gamma for an ideal gas.

We are interested in hotspot or isobaric ignition which means that just before ignition, the hotspot and cold fuel have nearly the same pressure, that is we can assume $P_c = P$. Using the expressions for the speeds of sound in equations 2.22, 2.25 and the assumption of pressure equilibrium allows us to rewrite the expression for the confinement time as:

$$\tau = \frac{R}{C_h}\left(1 + \frac{\Delta R}{R}\sqrt{\frac{\rho_c}{\rho}}\right) = \frac{R}{C_h}\left(1 + \frac{\rho_c \Delta R}{\rho R}\sqrt{\frac{\rho}{\rho_c}}\right) \tag{2.26}$$

Notice that rewritten this way, the confinement time in equation 2.26, looks like the confinement time of a bare hotspot times a factor greater than one which represents the extra confinement time due to the hydrodynamic tamping of the cold ice shell.

Again using the ideal gas law the speed of sound of the hotspot can be expressed as:

$$C_h = \sqrt{\frac{\gamma 2 N_0 K_B T}{\bar{A}}} \tag{2.27}$$

Inserting equations 2.26 and 2.27 back into equation 2.20 allows us to write an expression for ρRT^2.

$$\rho R T^2 > \frac{12}{T_\alpha}\sqrt{\frac{2\gamma A_{DT} K_B}{N_0}}\frac{T^{3.5}}{\langle\sigma v\rangle}\left\{\frac{1}{1+\frac{\rho_c \Delta R}{\rho R}\sqrt{\frac{\rho}{\rho_c}}}\right\}\left[\frac{\sqrt{0.8\chi_D + 1.2\chi_T}}{4\chi_D\chi_T}\right] \tag{2.28a}$$

The expression in the curly brackets represents the extra factor due to tamping. The expression in the square brackets is unity for an equimolar mixture of deuterium and tritium. Putting in the numbers for the conventional units gives:

$$\rho R T^2 > 5.06116 \times 10^{-19} \frac{T^{3.5}}{\langle \sigma v \rangle} \left\{ \frac{1}{1+\frac{\rho_c \Delta R}{\rho R}\sqrt{\frac{\rho}{\rho_c}}} \right\} \left[\frac{\sqrt{0.8\chi_D + 1.2\chi_T}}{4\chi_D \chi_T} \right] \tag{2.28b}$$

Numerical simulations indicate the best results are obtained by using the higher temperature fit to the thermonuclear reaction rate found in equation 2.9c, giving:

$$\rho R T^2 > \frac{12.6172}{T^{0.09}} \left\{ \frac{1}{1+\frac{\rho_c \Delta R}{\rho R}\sqrt{\frac{\rho}{\rho_c}}} \right\} \left[\frac{\sqrt{0.8\chi_D + 1.2\chi_T}}{4\chi_D \chi_T} \right] \tag{2.28c}$$

Just as Ricardo Betti did, it is convenient to define an ignition parameter which is a dimensionless ratio.

$$\beta = \frac{\rho R T^2}{5.06115 \times 10^{-19}} \frac{\langle \sigma v \rangle}{T^{3.5}} \left\{ 1 + \frac{\rho_c \Delta R}{\rho R}\sqrt{\frac{\rho}{\rho_c}} \right\} \left[\frac{4\chi_D \chi_T}{\sqrt{0.8\chi_D + 1.2\chi_T}} \right] > 1 \tag{2.29a}$$

$$\beta = \frac{\rho R T^2}{12.6172} T^{0.09} \left\{ 1 + \frac{\rho_c \Delta R}{\rho R}\sqrt{\frac{\rho}{\rho_c}} \right\} \left[\frac{4\chi_D \chi_T}{\sqrt{0.8\chi_D + 1.2\chi_T}} \right] > 1 \tag{2.29b}$$

Defined this way the ignition condition is simply that β must be greater than unity.

In section III, numerical simulations will demonstrate that that $\beta > 1$ is a valid ignition criterion and we will derive a simpler form for the tamping factor. In section V, realistic capsule simulations will demonstrate that χ, η, β and ITFX all perform very well as ignition parameters.

III. The Generalized Meldner Problem

In the late 1970's and early 1980's, Heiner Meldner was an ICF designer at the Lawrence Livermore National Laboratory (LLNL). He was trying to understand the thermonuclear ignition threshold for Laser Fusion designs. Meldner took an ICF simulation code, with all relevant physics turned on and mapped out the burn/no-burn ignition conditions for a 1 milligram bare sphere of DT plasma [Meldner 1981]. In the modern versions of Meldner's ignition condition used in this report, a calculation is scored as burned if the specific yield exceeds 10 MJ/mg. However ignition is usually so abrupt that almost any method of scoring ignition would give very similar results.

Meldner plotted the boundary between burn and no-burn regions on a graph with the initial areal density or ρR of the sphere on the horizontal axis and the initial ion temperature on the vertical axis. Figure 3.1 below shows a modern reproduction of Meldner's exercise using CALEICF with thermonuclear burn, multi-group radiation transport, electron thermal conduction and charged particle transport all turned on. Such ignition boundary plots in the plane of ρR and Tion quickly became known as *Meldner Curves* around Livermore.

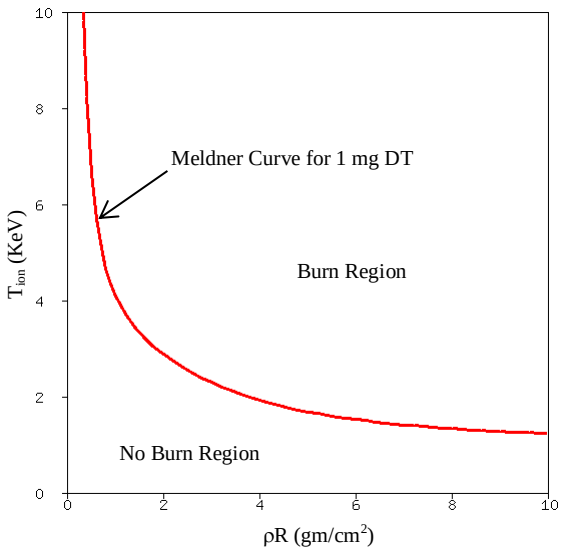

Figure 3.1: Modern reproduction of Heiner Meldner's calculation of the burn and no-burn regions of a 1mg bare sphere of DT plasma. Such ignition curves became known as *Meldner Curves* at LLNL.

The initial conditions of a bare sphere are completely specified by three numbers. The most obvious coordinate set would be initial density, initial temperature and initial radius. An equally acceptable coordinate set would be initial areal density or ρR, initial temperature and the mass of the sphere. A Meldner curve only plots the burn/no-burn boundary for a sphere of a single mass

and does not represent the ignition condition for the general case of all possible bare spheres of DT. However Meldner generated his ignition curves for bare DT spheres of several different masses and found that the ignition boundaries were not very sensitive to the mass but they were of course sensitive to the temperature and ρR of the sphere. Figure 3.2 shows three different Meldner curves for DT spheres with masses of 0.1 mg, 1.0 mg and 10 mg. The three curves are not identical but all three are very similar particularly in the region of ρR < 1 where most ICF hotspots operate.

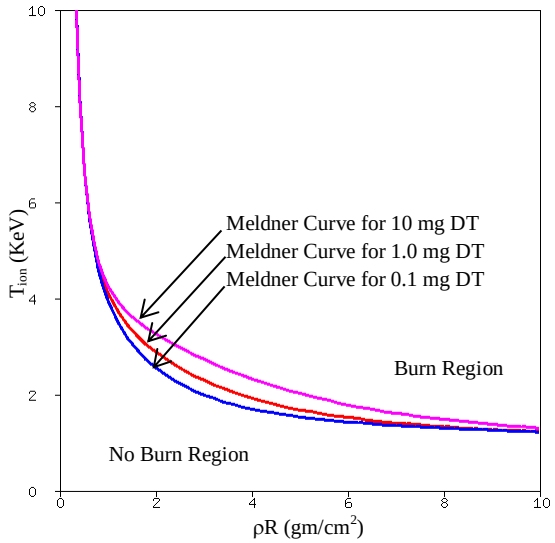

Figure 3.2: Meldner curves for 0.1 mg, 1.0 mg and 10 mg DT spheres. The ignition boundary does depend on the mass of the sphere, but the dependence on mass is not strong.

By the mid 1980's, it became common practice to use only the 1 mg Meldner curve and make the assumption that this was a universal ignition curve for any ICF hotspot. This approximation of using the 1 mg Meldner curve as the universal ignition threshold condition was championed mostly by Dick Doyas [Doyas 1984].

Meldner and Doyas did not specify a well-defined ignition condition analogous to the Lawson criterion instead they used the Meldner curve in a qualitative way which is illustrated in figures 3.3 and 3.4 with a modern NIF shot. The blue and red curves in figure 3.3 represent the calculated trajectories of the hot spot for NIF Shot N110620 in the space of ρR and Tion. Some care was taken so that the ρR and temperature in these plots represent the conditions for the hot spot and not averaged over the entire DT fuel. The blue curve represents the trajectory of a clean one dimensional calculation with thermonuclear reactions turn on (labeled Burn On). It is apparent that the clean one dimensional calculation of this shot ignites with a maximum hot spot temperature which is off scale at 100 KeV. The red curve represents the trajectory of a clean one dimensional calculation with thermonuclear reactions turned off (labeled Burn Off). The

magenta curve is the 1 mg Meldner curve. Notice that the burn-off trajectory does not cross the Meldner curve even though the burn-on calculation ignites. This apparent discrepancy is due to the inertial tamping effect of the cold fuel which was excluded from Meldner's bare sphere calculations.

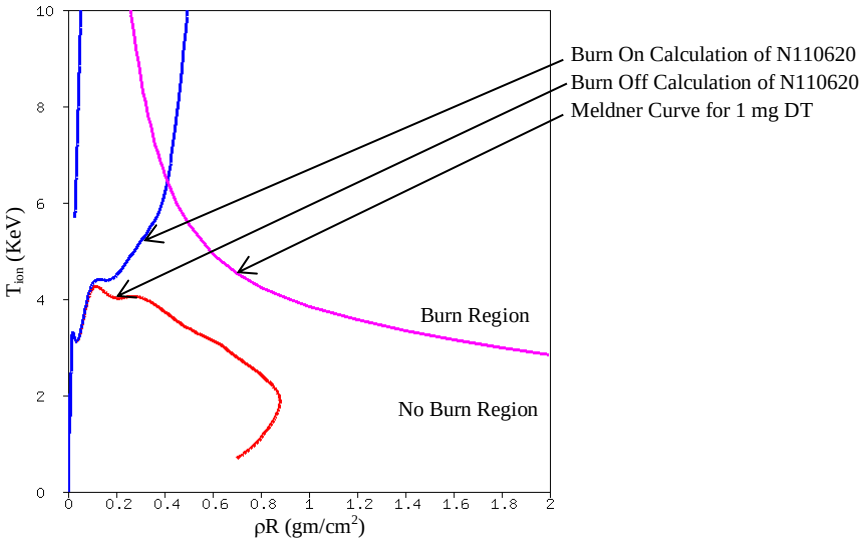

Figure 3.3: Meldner curve for a 1 mg DT sphere along with the calculated burn-on and burn-off trajectories of NIF shot N110620.

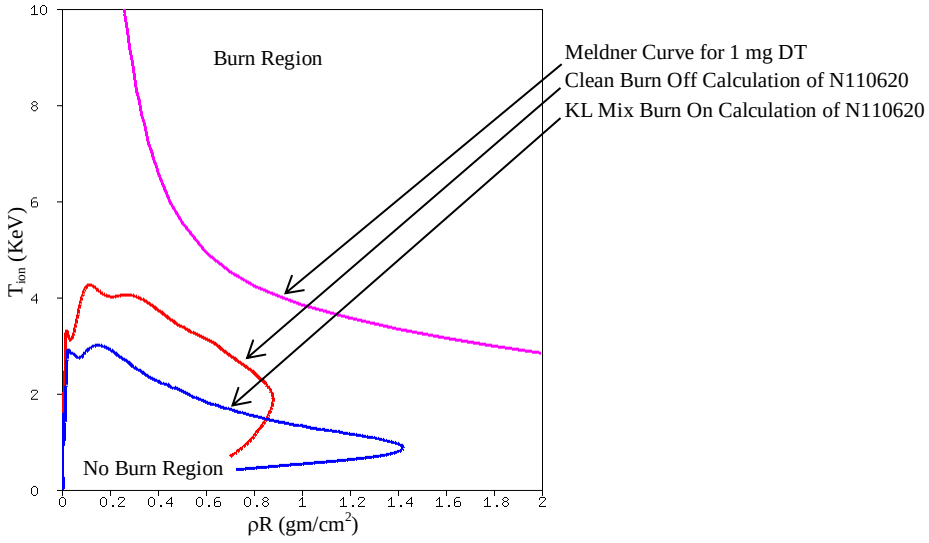

Figure 3.4: Meldner curve for a 1 mg DT sphere along with a clean burn-off calculation of NIF shot N110620 and a KL Mix burn-on calculation of shot N110620. With the mix model turned on, the hotspot trajectory falls even lower and the shot fails to ignite.

Meldner's philosophy was that in order to achieve robust ignition, the burn-off trajectory should not only cross the Meldner curve, but it should travel as far up into the burn region and as far away from the Meldner curve as possible. Meldner reasoned that real world degradations would lower the trajectory of the burn-off calculation and as a precaution the burn-off calculation needed to extend as far as possible beyond the ignition threshold represented by the Meldner curve.

Using this philosophy, which was popularized by Dick Doyas, both Meldner and Doyas would almost certainly reject the design for NIF Shot N110620 as being too marginal because the burn-off trajectory does not cross the Meldner curve. Figure 3.4 justifies their conservatism. In figure 3.4 once again the red curve is the trajectory of the clean one dimensional burn-off calculation, but the blue curve is the trajectory of a one dimensional calculation in which both burn and the KL turbulence mix model [Dimonte 2006] have been turned on. The details of the mix model are not very important here. Instead what is important is that shot N110620 is so marginal that almost any degradation such as those due to the turbulence model is sufficient to prevent the shot from igniting. This picture is consistent with reality because shot N110620 did not ignite.

Even though Meldner didn't do so, it is easy to turn Meldner's ignition curve into an ignition criterion. We start by fitting the Meldner curve to a power law:

$$\rho R T^n = Constant \tag{3.1}$$

If we take the log of equation (3.1) and rearrange we get:

$$log(\rho R) = log(Constant) - n log(T) \tag{3.2}$$

If we take the derivative of this expression we find:

$$n = -\frac{d(log(\rho R))}{d(log(T))} \tag{3.3}$$

Figure 3.5 shows the results of performing this procedure numerically on the Meldner curve for a 1mg bare DT sphere. The logarithmic derivative shows that there is no single temperature exponent which can match the Meldner curve over the entire temperature range. However for large temperatures (T > 6 KeV) which corresponds to small ρR (ρR < 1 gm/cm^2) the exponent that works best is approximately n = 1. For lower temperatures (T < 6 KeV) which corresponds to large ρR (ρR > 1 gm/cm^2) n = 2 is the exponent that works best.

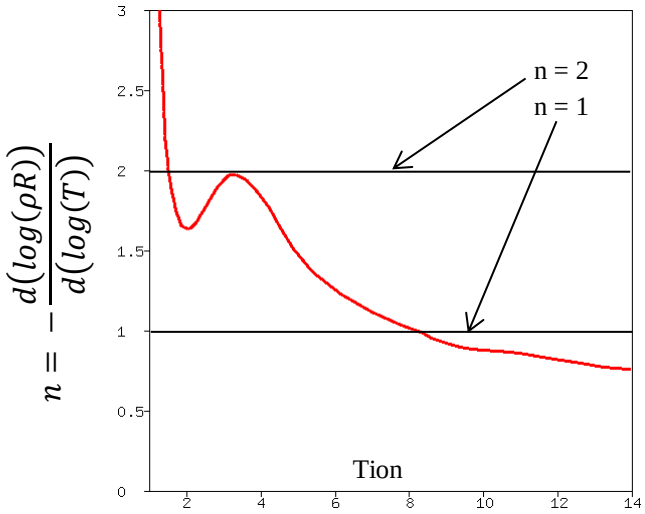

Figure 3.5: The logarithmic derivative of the 1 mg Meldner Curve shows there is no single temperature exponent which can represent the Meldner Curve over the entire range of temperatures, but for large temperatures > 6 KeV (and hence small ρR < 1) the exponent n = 1 works best while for small temperatures < 6 KeV (and hence ρR > 1) the exponent n = 2 works best.

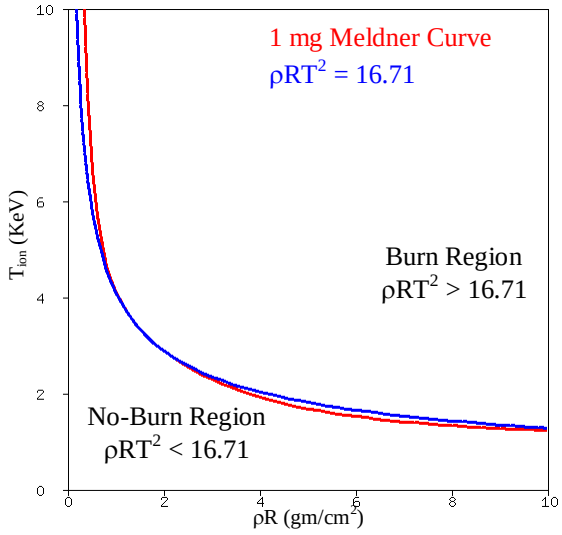

Figure 3.6: Simple fit to the Meldner curve. The red curve is the usual 1 mg Meldner curve. The blue curve is a plot of $\rho RT^2 = 16.71$. The two curves are not identical, but $\rho RT^2 = 16.71$ is a good approximation to the 1 mg Meldner curve.

A least squares power law fit to the 1mg Meldner curve is $\rho RT^{1.62} = 13.15$. However a quadratic power law of $\rho RT^2 = 16.71$ is a pretty close approximation to the 1mg Meldner curve and is generally more convenient to use. This close match is displayed in figure 3.6. The red curve is the standard 1mg Meldner Curve. The blue curve is a plot of the equation $\rho RT^2 = 16.71$. The two

curves are not identical but they are very close. Notice how the curve where $\rho RT^2 = 16.71$ divides the ρR – Tion plane into two distinct regions: The lower left area with $\rho RT^2 < 16.71$ which is nearly identical to the no-burn region below the Meldner curve and the upper right area with $\rho RT^2 > 16.71$ which is nearly identical to the burn region above the Meldner curve.

Figure 3.6 demonstrates that Meldner's ignition criteria which required the burn-off trajectory of the hotspot in ρR – Tion space to cross over the Meldner curve to a very good approximation can be restated simply as the requirement that the maximum value of ρRT^2 for the hot spot in a burn-off calculation must exceed 16.71 gm-KeV^2/cm^2. Furthermore, Meldner's assertion that the most robust ICF capsule will occur when the burn-off trajectory of the hot spot is as far above the Meldner curve as possible is the same as requiring the maximum value of ρRT^2 in the hot spot be as large as possible.

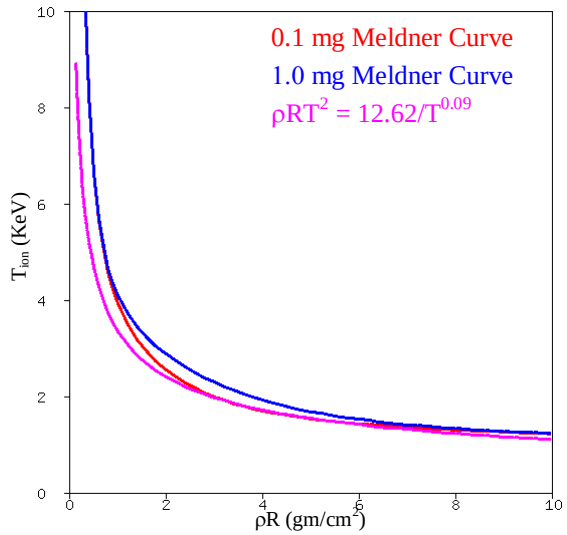

Figure 3.7: Comparison of Meldner curves for DT masses of 0.1 and 1.0 mg with the analytic approximation of section II. The red curve is the Meldner curve for a bare DT mass of 0.1mg. The blue curve is the Meldner curve for a bare DT mass of 1.0 mg. The magenta curve is $\rho RT^2 = 12.62/T^{0.09}$ which is the bare DT sphere limit of equation 2.28c in section II. The analytic model does not match either numerically generated Meldner curve, but comes close to matching the 0.1 mg ignition curve.

Figure 3.7 compares the numerically generated Meldner curves for bare DT spheres with the analytic expression derived in section II. The red curve in figure 3.7 is the Meldner curve for a bare DT sphere of 0.1 mg and the blue curve is the Meldner curve for a DT mass of 1.0 mg. The magenta curve is a plot of equation 2.28c in section II taken in the limit of no tamping. The analytic model does not exactly match either numerically generated ignition condition, but it comes close to matching the ignition boundary for the 0.1 mg bare DT sphere. Figure 3.7 is

confirmation that Lawson's ignition hypothesis (equation 2.1 in section II) and the approximation that the confinement time is just the speed of sound transit time across the hotspot (equation 2.21) are reasonably accurate assumptions at least in the case of the bare DT sphere because the analytic model and the numerical models are in general agreement.

Note that Meldner's calculations of bare DT spheres made no attempt to account for the hydrodynamic tamping of the cold DT fuel which should be present in a healthy ignition capsule. The effect of tamping is significant. This is the reason why a clean calculation of NIF shot N110620 was able to ignite even though the no-burn trajectory never crossed the Meldner curve.

However in defense of Meldner, I don't think he left out tamping out of ignorance. Instead he wanted to be cautious. If the burn-off trajectory of an ICF hot spot crossed over the Meldner curve which ignored tamping, then in reality the hotspot would have some extra margin which is usually a good thing. That extra margin would make the design more robust against all of the various degradation mechanisms that have been imagined and perhaps some that haven't been imagined.

On the other side of the argument, in order for a NIF design to achieve a maximum burn-off value for ρRT^2 of 16.71 gm-KeV^2/cm^2, the implosion velocity must be very high – approaching 400 km/sec. NIF implosions reaching those speeds demand very high accelerations and also require that almost all of the ablator be burned off leading to a very high risk of failure due to Rayleigh-Taylor instabilities at the ablation front.

Meldner Curves with Tamping

Meldner's bare DT sphere problem can be generalized by surrounding the hotspot with a spherical layer of cold DT ice. Recall that it takes three numbers to describe a bare DT sphere: the initial areal density, ρR, initial temperature, T, and the mass. In the generalization proposed here, Meldner's bare sphere will become the hotspot and so we will still need a triplet of numbers to describe the initial state of the hotspot, however we will need another set of three numbers to describe the cold shell of DT ice. This second triplet could be the initial pressure, the initial density and the mass of the cold shell. Of these three numbers, the pressure can be eliminated, because for hotspot ignition, the hotspot and cold shell are nearly in pressure equilibrium just before ignition. Hotspot ignition is sometimes known as isobaric ignition for this reason as opposed to the isochoric case appropriate for fast ignition.

So once the ρR, temperature and mass of the hotspot are given, the pressure of the hotspot is fixed and we will assume that the cold shell is initialized with the very same pressure. That still leaves two new degrees of freedom: the density of the shell and the mass of the shell, which are combined with the three numbers used to describe the initial state of the hotspot for a total of five

numbers to describe the initial state of any calculation. It is convenient to rearrange these five numbers a little bit so that our final parameter list for the specification of the generalized Meldner problem is:

1) The initial areal density of the hotspot – ρR.
2) The initial temperature of the hotspot – T.
3) The total mass of both hotspot and cold shell – M_{DT}.
4) The mass fraction of the hotspot – M_f.
5) The ratio of the cold shell pressure to the degeneracy pressure – α.

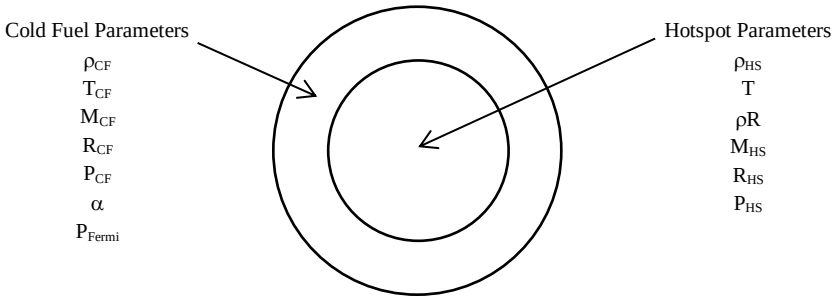

Figure 3.8: Initial conditions for generalized Meldner calculations.

Given these 5 parameters, the procedure for establishing the initial conditions for the hotspot and cold shell are listed below:

1) Find the mass of the hotspot – $M_{HS} = M_f M_{DT}$.
2) Find the radius of the hotspot – $R_{HS} = \sqrt{3M_{HS}/(4\pi\rho R)}$.
3) Find the density of the hotspot – $\rho_{HS} = \rho R / R_{HS}$.
4) Find the pressure of the hotspot – $P_{HS} = 2N_0 K_B \rho_{HS} T / A_{DT}$.
5) Find the pressure of the cold fuel – $P_{CF} = P_{HS}$.
6) Find the degeneracy pressure in the cold fuel – $P_{Fermi} = P_{CF}/\alpha$.
7) Find the density of the cold fuel – $\rho_{CF} = \left[\frac{P_{Fermi}}{2.1576}\right]^{3/5}$.
8) Find the temperature of the cold fuel – $T_{CF} = \{Inverse\ EOS\ lookup\}(\rho_{CF}, P_{CF})$.
9) Find the mass of the cold fuel – $M_{CF} = \left(1 - M_f\right)M_{DT}$.
10) Find the outer radius of the cold fuel – $R_{CF} = [R_{HS}^3 + 3M_{CF}/(4\pi\rho_{CF})]^{1/3}$.

Finding the boundary which separates the region that ignites from the region that fails to ignite in a five dimensional space is a daunting task and somewhat difficult to visualize. However after a few initial calculations it quickly became apparent that the ignition surface is extremely insensitive to the total DT mass. This is analogous to Meldner's earlier hypothesis that the

ignition curve is insensitive to the total mass of the bare DT sphere only in these tamped calculations this approximation is even more accurate. However tamped calculations also demonstrate that the ignition surface does depend on the mass fraction of the hotspot. Calculations also indicate that the ignition boundary is very insensitive to the degeneracy parameter α. This means that we only have to search a three dimensional space ($\rho R, T, M_f$) for the ignition surface rather than a five dimensional space ($\rho R, T, M_f, M_{DT}, \alpha$) .

Once the total mass, M_{DT}, the degeneracy ratio, α, and the hotspot mass fraction, M_f, are selected, the problem is reduced to finding the ignition curve in the plane of initial temperature and areal density much like Meldner's original work. Figure 3.9 shows 7 ignition curves for a range of hotspot mass fractions given a total DT mass of 0.200 milligrams and a degeneracy ratio of $\alpha = 2.0$. Once again CALEICF was used in one dimension with all relevant physics turned on to perform the calculations and once again a calculation was scored as ignited if the specific yield of the hotspot exceeded 10 MJ/mg. Note that a hotspot mass fraction of 1.00 means that all of the mass is in the hotspot and the mass of the cold fuel is zero. Such a situation corresponds to Meldner's bare DT mass of 0.200 mg.

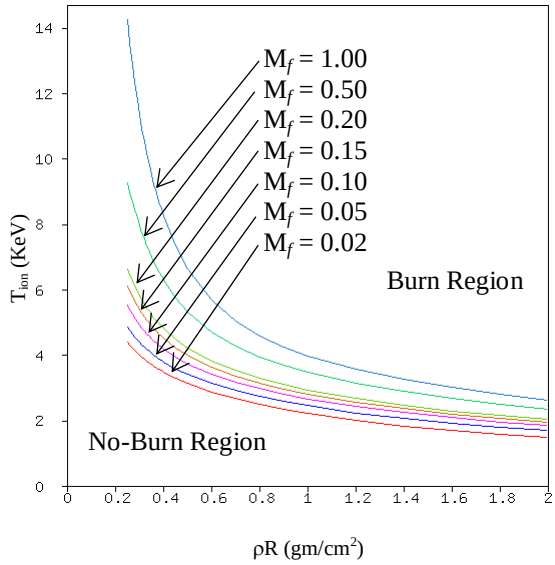

Figure 3.9: Tamped ignition curves for M_{DT} = 0.200 mg, $\alpha = 2.0$ and hotspot mass fractions, M_f, of 0.02, 0.05, 0.10, 0.15, 0.20, 0.50 and 1.00. Note that a hotspot fraction of 1.00 corresponds to one of Meldner's bare DT mass ignition curves.

It may not be obvious, but a close examination of figure 3.9 reveals that $1 - M_f$ tracks the degree of inertial tamping due to the cold fuel. Obviously with a hotspot mass fraction of 1, or $1 - M_f = 0$, there is no cold fuel and therefore no tamping. As the hotspot mass fraction decreases, there is relatively more cold fuel mass compared to the hotspot mass and the degree of inertial

tamping increases which causes the ignition curves in figure 3.8 to slide progressively downward to lower temperatures as the hotspot mass fraction gets smaller.

One might look at figure 3.9 and take away the conclusion that a good strategy for an ICF design would be to make the hotspot mass fraction as small as possible because then the required ignition temperature could be made rather low. However, one reason the small hotspot mass fraction calculates to ignite so easily is because it takes a lot of spherical convergence to get a small hotspot mass up to the ρR's needed for ignition. For the 2% mass fraction ignition curve in figure 3.9, the radius of the hotspot with a ρR of 0.5 gm/cm^2 is only 13.8 microns. When the ρR gets to 1.0 gm/cm^2, the hotspot radius needed is 9.8 microns. Both of these radii represent huge convergence ratios of 80 and 112 respectively. Such extreme convergence ratios would be very hard to achieve in reality.

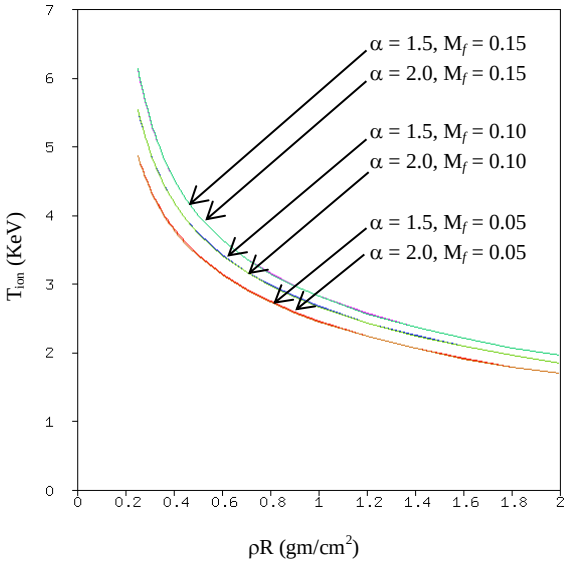

Figure 3.9a

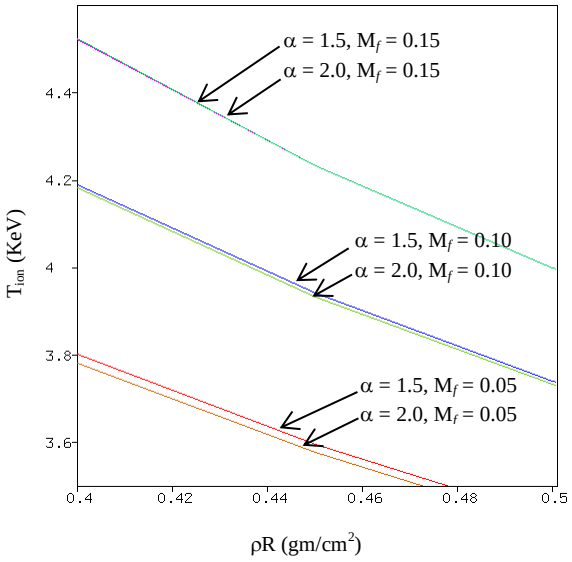

Figure 3.9b

Figure 3.10: Six ignition curves for M_{DT} = 0.200 mg. The 6 cases are (1) α = 2.0, M_f = 0.05; (2) α = 2.0, M_f = 0.10; (3) α = 2.0, M_f = 0.15; (4) α = 1.5, M_f = 0.05; (5) α = 1.5, M_f = 0.10 and (6) α = 1.5, M_f = 0.15. Figure 3.9a shows the ignition curves over their full range of ρR and temperature where the α = 2.0 curves and the α = 1.5 curves appear to overlay each other. Figure 3.9b shows the ignition curves over a restricted range of ρR and temperature and the slight sensitivity to α is just visible.

Figure 3.10 shows the effect of different degeneracy ratios. Both figures 3.10a and 3.10b plot 6 different ignition curves but in figure 3.10a only 3 curves are visible. This is because the α = 2.0 curves and the α = 1.5 curves are so close to each other that they are nearly indistinguishable. Figure 3.10b shows a blowup of the same 6 curves and it is just possible to see the separation

between $\alpha = 1.5$ and $\alpha = 2.0$ for the $M_f = 0.05$ and $M_f = 0.10$ cases but the curves for the $M_f = 0.15$ are still on top of each other. The main point to take away from figure 3.10 is that the ignition curves of these tamped hotspot calculations are largely insensitive to the pressure degeneracy ratio α.

Figure 3.11 shows the ignition curves for 3 different values of the total DT mass. All 3 cases have the same value of the degeneracy ratio, $\alpha = 2.0$, and the hotspot mass fraction $M_f = 0.10$. There is a small visible difference between the three ignition curves but the difference is very small – much smaller than the difference in ignition curves seen for the bare DT sphere case in figure 3.2. The main point of figure 3.11 is that the ignition surface is nearly insensitive to the total mass of the DT fuel.

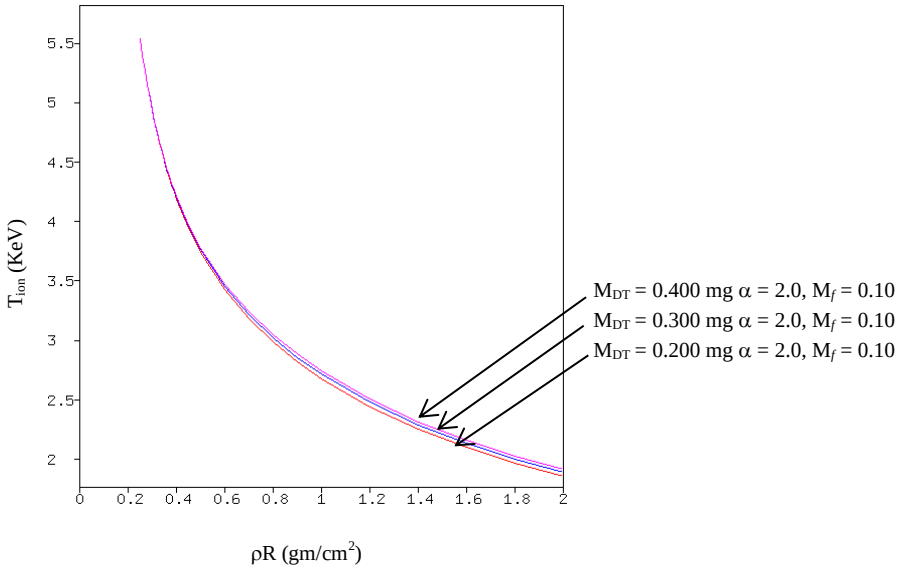

Figure 3.11: Ignition curves for 3 different DT masses: (1) $M_{DT} = 0.200$ mg, $\alpha = 2.0$, $M_f = 0.10$; (2) $M_{DT} = 0.300$ mg, $\alpha = 2.0$, $M_f = 0.10$ and (3) $M_{DT} = 0.400$ mg, $\alpha = 2.0$, $M_f = 0.10$. Ignition curves depend on hotspot fraction, but are insensitive to total DT mass.

Let us return to the ignition curves in figure 3.9. Is there a simple analytic form that accurately summarizes the numerically generated curves in figure 3.9? It's easy to fit each curve individually to a simple power law of the form $\rho R T^n = C$. Table 3.1 lists the results of performing a least squares fit for each of the curves in figure 3.9.

Table 3.1: Power Law Fits for each Curve	
Hotspot Mass Fraction M_f	Fit
$M_f = 0.02$	$\rho RT^{1.9753} = 4.7346$
$M_f = 0.05$	$\rho RT^{2.0281} = 6.0794$
$M_f = 0.10$	$\rho RT^{1.9547} = 6.7531$
$M_f = 0.15$	$\rho RT^{1.8658} = 6.9026$
$M_f = 0.20$	$\rho RT^{1.7877} = 6.9102$
$M_f = 0.50$	$\rho RT^{1.5139} = 6.8676$
$M_f = 1.00$	$\rho RT^{1.2208} = 5.6305$

Each of these individual fits matches their respective curves with small fitting errors. Note that the exponents of these fits smoothly vary from around 2 for small hotspot mass fractions to 1.22 for a mass fraction of 1. The constants, C, also vary in a systematic way with respect to the mass fraction. One could try to fit both the sequence of exponents and constants as a function of the hotspot mass fraction. However such an arrangement would be cumbersome. It is more convenient to look for an overall fit in which the temperature exponent is the same for all mass fractions. To this end we will search for a fit for all ignition curves of the following form:

$$\rho RT^n = AM_f^P \tag{3.4}$$

Taking the logarithm of equation 3.4 produces an expression in which all of the free parameters appear in a linear relationship.

$$nlog(T) + log(\rho R) = Plog\left(M_f\right) + log(A) \tag{3.5}$$

Equation 3.5 was fit to the data in figure 3.9 by finding the least squared residual error. However the quality of the fit wasn't very good particularly for mass fractions less than 0.20 which is the area of greatest interest for NIF ignition designs. A second least squares fit of equation 3.5 was made to the numerical ignition curves in figure 3.9, the difference being that this second fit was restricted to the ignition curves with mass fractions less than or equal to 0.20. The resulting least squares fit is listed below:

$$\rho RT^{1.9} = 12.068M_f^{0.2689} \qquad \text{RMS error 2.7\%} \tag{3.6}$$

The RMS error for this fit was very good at 2.7%.

The exponent which minimizes the RMS error is 1.9 which is very close to 2.0. Since a lot of work had already been with the ignition parameter ρRT^2, a third least squares fit was performed in which the temperature exponent was fixed at 2.0. The resulting fit was:

$$\rho RT^{2.0} = 14.2478 M_f^{0.2831} \qquad \text{RMS error 3.4\%} \qquad (3.7)$$

The RMS error for this n = 2 fit was only slightly greater at 3.4% than the error for the n = 1.9 fit which had an error of 2.7%. Notice that if we set M_f to 1.0 in equation 3.7, we get an estimate of the ignition curve for a bare sphere which is:

$$\rho RT^{2.0} = 14.2478 \qquad (3.8)$$

Compare equation 3.8 above with the fit to the Meldner curve found earlier in this section. Figure 3.6 shows that a good approximation to the 1mg Meldner curve is:

$$\rho RT^2 = 16.71 \qquad (3.9)$$

We can compare both of these ignition curves to equation 2.28c in section II taken in the limit of no tamping and an equimolar fuel:

$$\rho RT^2 = 12.62/T^{0.09} \qquad (3.10)$$

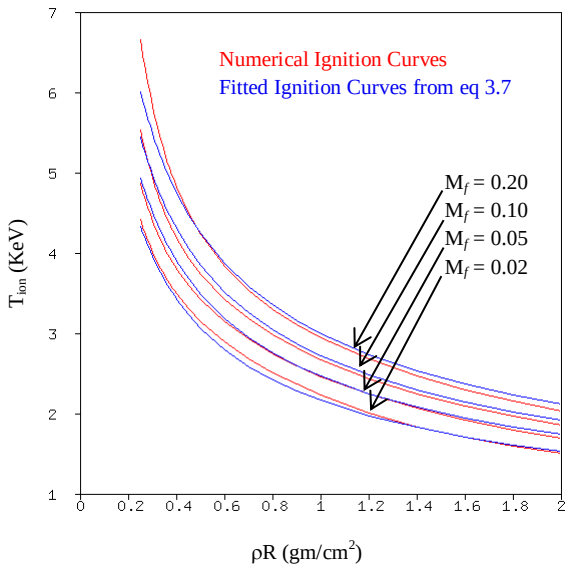

Figure 3.12: Comparison between the numerical ignition curves (in red) and the fits generated by equation 3.7 (in blue). The numerical curves all have a total DT mass of 0.200 mg and degeneracy pressure ratio of $\alpha = 2.0$. The match is not perfect but good enough to show that equation 3.7 is a useful approximation.

Thus we see that the analytic approximations made in section II and the numerical results of section III are largely in agreement at least in the untamped limit of a bare DT sphere.

The more interesting question is how well does equation 3.7 fit the numerical results in the more realistic case of a tamped hotspot. Figure 3.12 compares the numerical ignition curves with the fits coming from equation 3.7. The agreement isn't perfect but it's still very good. The main point of this comparison is to show that equation 3.7 is an accurate representation of the numerically generated ignition threshold for the ρRT^2 ignition criterion.

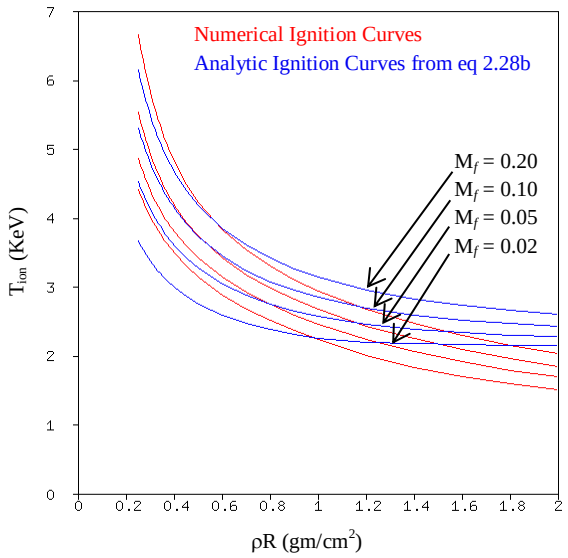

Figure 3.13: Comparison between the numerical ignition curves (in red) and the analytic model in equation 2.28b (in blue). The numerical curves all have a total DT mass of 0.200 mg and degeneracy pressure ratio of $\alpha = 2.0$. The match is not is as good as the fit expressed in equation 3.7 and plotted in figure 3.12

The final question of this section is how well does the analytic ignition condition found in section II and represented by equation 2.28 match with the numerical results found in this section? Recall that equation 2.28 comes in two forms: equation 2.28b which expresses the ignition threshold in terms of the thermonuclear reaction rates $\langle\sigma v\rangle$ which have to be looked up in a table:

$$\rho RT^2 > 5.06115 \times 10^{-19} \frac{T^{3.5}}{\langle\sigma v\rangle} \left\{ \frac{1}{1+\frac{\rho_C \Delta R}{\rho R}\sqrt{\frac{\rho}{\rho_C}}} \right\} \left[\frac{\sqrt{0.8\chi_D + 1.2\chi_T}}{4\chi_D\chi_T} \right] \qquad (2.28b)$$

and equation 2.28c which replaces <σv> with a power law approximation to give a closed-form expression for the ignition condition:

$$\rho R T^2 > \frac{12.6172}{T^{0.09}} \left\{ \frac{1}{1+\frac{\rho_c \Delta R}{\rho R}\sqrt{\frac{\rho}{\rho_c}}} \right\} \left[\frac{\sqrt{0.8\chi_D + 1.2\chi_T}}{4\chi_D \chi_T} \right] \qquad (2.28c)$$

Figure 3.13 plots the numerical ignition condition found by solving the generalized Meldner problem for four different hotspot mass fractions against the ignition condition implied by equation 2.28b. Figure 3.14 plots the numerical ignition condition against those implied by equation 2.28c.

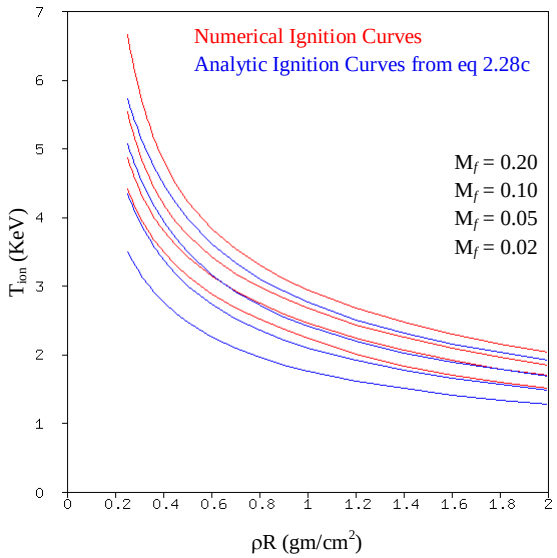

Figure 3.14: Comparison between the numerical ignition curves (in red) and the analytic model in equation 2.28c (in blue). The numerical curves all have a total DT mass of 0.200 mg and degeneracy pressure ratio of α = 2.0. The match is not is as good as the fit expressed in equation 3.7 and plotted in figure 3.12

There isn't any question that the ignition conditions found by numerical simulations are in some sense the right answer. Yes we have made many simplifying assumptions such as spherical symmetry and uniform spatial conditions within the hotspot and cold fuel but beyond those simplifications which actually define the problem no addition approximations of any significance have been made. The analytic ignition condition expressed by equation 2.28b is based upon the starting assumption of Lawson expressed in equation 2.1 which assumes that ignition will occur when the thermonuclear heating rate exceeds a critical rate related to the speed of sound transit time across the cold fuel and hotspot. Those are assumptions which are only approximately true.

The discrepancies between the red and blue curves in figures 3.13 and 3.14 illustrate the quality of those assumptions.

Figure 3.13 compares the numerical ignition conditions with equation 2.28b which should be more accurate than equation 2.28c because no approximation is made for the thermonuclear rates. There is a rough correspondence between the numerical and analytic ignition curves particularly for the lower hotspot ρR's. However sizable discrepancies exist for larger hotspot ρR's. This suggests that Lawson's fundamental assumption about ignition expressed in equation 2.1 is a good assumption for low ρR and not so good at larger ρR's.

Figure 3.14 compares the numerical ignition conditions with equation 2.28c which should be less accurate than equation 2.28b because the tabular TN reaction rates have been replaced with a power law approximation. At first glance the analytic curves in figure 3.14 appear somewhat better matched to the numerical curves than what we saw in figure 3.13. This is misleading. Figure 3.14 looks better because of compensating errors. The details of the power law fit for the TN reaction rates were intentionally chosen so that the temperature exponent in the ignition condition would be close to 2. This was done with full knowledge that an exponent of 2 would give a decent match to the numerical results. By choosing an imperfect fit to the TN rates, we have partially balanced the error of the fit to the TN rates against the errors in Lawson's principal assumption.

The analytic ignition condition embodied in equation 2.28 is attractive because it is so easily derived, but the fit to the solution to the generalized Meldner found in equation 3.7 is both easier to use (because you don't need to find the density ratio or the areal density ratio of the hotspot to cold fuel) and equation 3.7 is ultimately more accurate because it is a good fit to numerical simulations which solve the ignition problem without invoking Lawson's principal hypothesis.

IV. Experimental Measurement of Ignition Parameters

It is possible to infer the values of the ignition figures-of-merit directly from the data taken on a NIF shot without resorting to code simulations. The methodology adopted in this section was first proposed by Paul Springer and Charlie Cerjan [Springer 2011]. The fundamental assumption is that the yield of the capsule can be expressed as a function of the basic properties of the hotspot.

$$Y_n = n_{ion}^2 \chi_D \chi_T \langle \sigma v(T) \rangle \tau \frac{4\pi}{3} R_{HS}^3 \tag{4.1}$$

Y_n is the D+T neutron yield of the shot. The average ion number density of the hot spot is n_{ion}. The symbols χ_D and χ_T are the deuterium and tritium atom fractions which are usually set to 0.5. The Maxwell averaged thermonuclear cross section multiplied by the ion velocity for the DT reaction at temperature T is $<\sigma v>$. The burn duration is τ and the hot spot radius is R_{HS}. All of these values can be measured directly except for the average ion number density.

The average temperature, T, of the hot spot is inferred from the neutron time-of-flight (NTOF) spreading. The burn duration, τ, is taken to be the full-width half-maximum of the thermonuclear gamma reaction history signal. The radius of the hot spot, R_{HS}, is taken to be the P_0 component of the 17% contour of the neutron pin-hole image and of course the neutron yield, Y_n, is taken from the neutron detectors.

Equation 4.1 above can be inverted to solve for the ion number density:

$$n_{ion} = \sqrt{\frac{3Y_n}{4\pi \chi_D \chi_T \langle \sigma v(T) \rangle \tau R_{HS}^3}} \tag{4.2}$$

Equation 4.2 expresses the ion number density in terms experimentally accessible quantities. With this expression for the number density we can get to the other quantities of interest.

First we find an expression for ρRT^2:

$$\rho RT^2 = Scale \left(\frac{An_{ion}}{N_0}\right) T^2 R_{HS} = \frac{A}{N_0} \sqrt{\frac{3}{4\pi \chi_D \chi_T}} \sqrt{\frac{Y_n}{\tau R_{HS}}} \left(\frac{T^2}{\sqrt{\langle \sigma v \rangle}}\right) \tag{4.3a}$$

$$\rho RT^2 = 4.081181 \times 10^{-10} Scale \sqrt{\frac{Y_n(10^{15})}{\tau(ns) R_{HS(\mu m)}}} \left(\frac{T^2}{\sqrt{\langle \sigma v(T) \rangle}}\right) \tag{4.3b}$$

In the last expression, ρRT^2 has units of gm-KeV^2/cm^2. Y_n has units of 10^{15} neutrons, τ has units of nanoseconds and R_{HS} has units of microns, T has units of kilovolts and $<\sigma v>$ is in units of cm^3/seconds. A = 2.515076 is the average atomic mass of the D+T mixture. N_0 is Avogadro's

number. Lastly we have assumed $\chi_D = \chi_T = 0.5$. The scale factor – *Scale* – will be determined shortly such that the experimental values of ρRT^2 will closely conform to the edit of ρRT^2 taken from our ICF codes.

Recall that for temperatures between 3 and 4.2 kilovolts, the Maxwell averaged reaction rate for the D+T reaction can be approximated as:

$$\langle \sigma v \rangle (\mathrm{cm}^3/\mathrm{sec}) = 2.216 \times 10^{-20} T^{4.01} \text{ with T in KeV} \tag{4.4}$$

Inserting equation 4.4 into 4.3b gives:

$$\rho RT^2 = 2.741\, Scale \sqrt{\frac{Y_n(10^{15})}{\tau(ns) R_{HS(\mu m)}}}\, T^{-0.005} \tag{4.5}$$

Equation 4.3b should be good for any hot spot temperature, whereas equation 4.5 should only be used for neutron time-of-flight temperatures between 3 and 4.2 kilovolts. Either expression can be used to take the experimental values for Y_n, τ, R_{HS} and T and turn them into an inferred value for ρRT^2.

Notice in the temperature range between and 3 and 4.2 kilovolts, the experimentally inferred value for ρRT^2 loses almost all dependence on temperature. This is because $<\sigma v>$ is nearly proportional to T^4 and the square root of that cancels the T^2 in the numerator.

Historically ρRT^2 along with ρR and ρRT has been edited by ICF codes by performing line integrals along a radial line:

$$\rho R = \int \rho_{DT} dr \tag{4.6a}$$
$$\rho RT = \int \rho_{DT} T dr \tag{4.6b}$$
$$\rho RT^2 = \int \rho_{DT} T^2 dr \tag{4.6c}$$

Each of the integrals cover the entire range of radii, but the density in the integrand is limited to the partial density of deuterium plus the partial density of tritium so the three integrals are associated with the entire compliment of thermonuclear fuel in the capsule and not limited to either the hot spot fuel or the cold fuel ice. Note that in those calculations in which the ablator material is allowed to mix with the DT fuel, the partial density of the ablator is specifically excluded from the definitions listed in equations 4.6a, 4.6b and 4.6c. In discussions referring to ρRT^2 as an ignition parameter the actual value used is the maximum in time of the instantaneous integral defined by equation 4.6c, in a calculation in which thermonuclear reactions have been turned off or the alpha energy depositions have been disabled.

These definitions for ρR, ρRT and ρRT^2 may be extended to two or three dimensions by taking the line integrals described in equations 4.6a, 4.6b and 4.6c along radial lines in many different directions and then forming an average where each radial integral is weighted by the appropriate solid angle fraction.

The question naturally arises, how does the code's internal edit of ρRT^2 compare with the inferred value represented by equation 4.3b or 4.5? What value for the *Scale* factor in equations 4.3 and 4.5 will give the best match to the ρRT^2 edit of an ICF code? To this end a series of simulations were performed of an ICF capsule which is similar, but not identical to the Revision 5 design tested at the National Ignition Facility (NIF). This is the same ICF design and the same series of calculations featured in section V. The design has an ablator made of plastic (CH) and doped with silicon.

In the series of calculations using this CH capsule, the temperatures of the foot along with the temperatures of the second, third and main pulses were randomly varied both up and down. The thermonuclear reactions were turned on but the resulting neutrons and alpha particles were not permitted to deposit any energy back into the plasma. Such simulations are usually known as no-alpha calculations. As we will see in section V, some of the variations in drive are severe enough to prevent the capsule from igniting even if the alpha energy had been deposited. Yet other drive variations are mild enough that the capsule would ignite. Thus we expect the range of ρRT^2 values to cover the region of the ignition threshold.

For each variation of the drive, the code's internal edit of ρRT^2 (the maximum in time of equation 4.6c) was recorded along with the experimentally inferred value (equation 4.3b with *Scale* = 1). The results are plotted in figure 4.1. Notice that to a high degree of accuracy the two versions of ρRT^2 are proportional to one another. A linear least squares fit of the points in figure 4.1 shows that the code's ρRT^2 is approximately 1.3174 times the measurement inferred by equation 4.3b. The RMS error of this simple fit is 0.9% and the maximum error is 3.7%.

Several different NIF designs have studied in this manner and the least squares fit between the code's version of ρRT^2 using the maximum of equation 4.6c and the experimentally inferred ρRT^2 using equation 4.3b with alpha depositions off always result in a coefficient of proportionality between 1.28 and 1.32. Therefore it is convenient to define the experimentally inferred value for ρRT^2 with a scale factor of 1.3 in equations 4.3 and 4.5:

$$\rho RT^2 = 1.3 \times \left(\frac{An_{ion}}{N_0}\right) T^2 R_{HS} = \frac{A}{N_0}\sqrt{\frac{3}{4\pi\chi_D\chi_T}}\sqrt{\frac{Y_n}{\tau R_{HS}}}\left(\frac{T^2}{\sqrt{\langle\sigma v\rangle}}\right) \tag{4.7a}$$

$$\rho RT^2 = 1.3 \times 4.081181 \times 10^{-10}\sqrt{\frac{Y_n(10^{15})}{\tau(ns)R_{HS(\mu m)}}}\left(\frac{T^2}{\sqrt{\langle\sigma v(T)\rangle}}\right) \tag{4.7b}$$

$$\rho RT^2 = 1.3 \times 2.741 \sqrt{\frac{Y_n(10^{15})}{\tau(ns) R_{HS(\mu m)}}}\, T^{-0.005} \qquad (4.7c)$$

In future sections of this report, when reference is made to the experimentally inferred values of ρRT^2, the scale factor of 1.3 will be included in the definition used for ρRT^2.

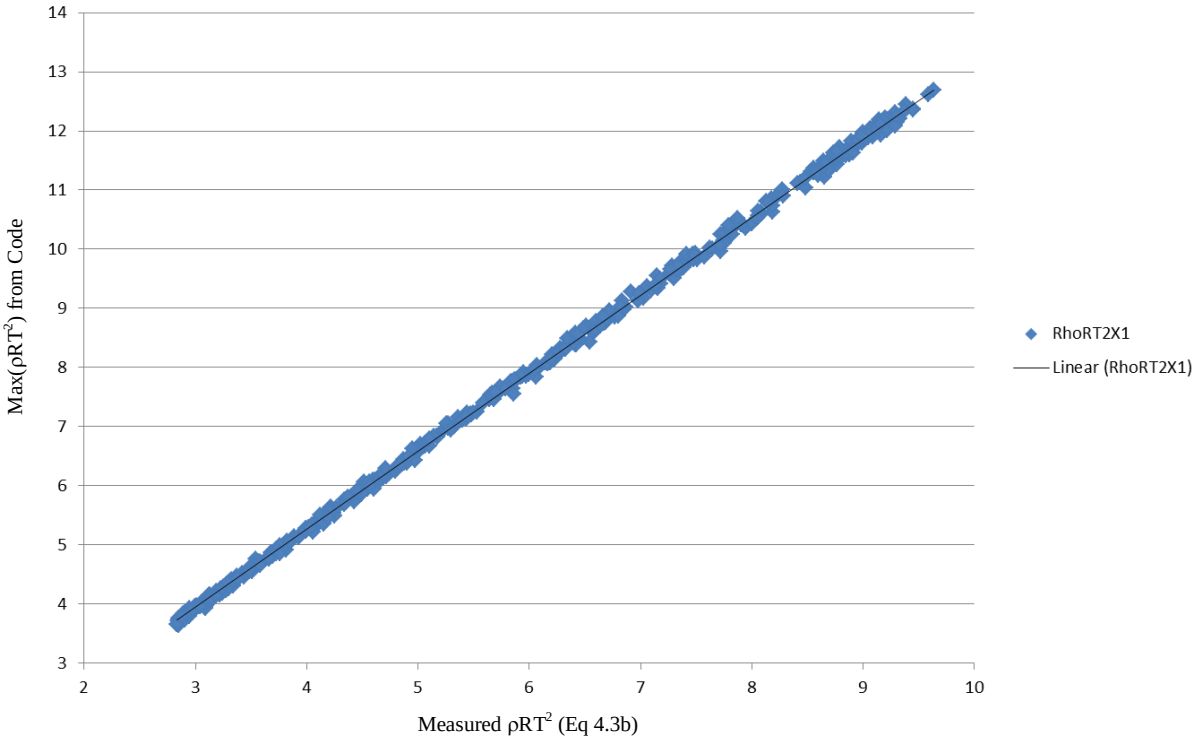

Figure 4.1: The blue diamonds compare the experimentally inferred ρRT^2 using equation 4.3b and ρRT^2 taken directly from the code run (the max of eq. 4.6c). The line is a least squares fit with a slope of 1.3174. The RMS error of the linear fit is 0.9%. The largest error is 3.7%.

In order to use ρRT^2 as part of an ignition criterion, we will also need an expression for the mass of the hotspot:

$$M_{HS} = \frac{4\pi}{3} R_{HS}^3 \rho_{HS} = \frac{4A}{N_0} \sqrt{\frac{\pi}{3}} \sqrt{\frac{Y_n R_{HS}^3}{\tau <\sigma v>}} \qquad (4.8a)$$

$$M_{HS}(\mu g) = 1.7095 \times 10^{-11} \sqrt{\frac{Y_n(10^{15}) R_{HS}^3(\mu m)}{\tau(ns) <\sigma v> (cm^3/sec)}} \qquad (4.8b)$$

In equation 4.8b the mass of the hotspot is in micrograms, Yn is divided by 10^{15}, R_{HS} has units of microns, τ has units of nanoseconds and $<\sigma v>$ has units of cm^3/sec. Substituting the power law fit to the TN reactions of equation 4.4 into equation 4.8b gives an approximate form for the mass of the hotspot:

$$M_{HS}(\mu g) = \frac{0.11484}{T^{2.005}} \sqrt{\frac{Y_n(10^{15}) R_{HS}^3(\mu m)}{\tau(ns)}} \tag{4.8c}$$

We can combine the expression for ρRT^2 in equation 4.7b or 4.7c with the ignition threshold we found from solving the generalized Meldner problem in section III (equation 3.7) to form the β ignition parameter:

$$\beta = \frac{\rho R T^2}{14.2478 M_f^{0.2831}} = 3.72372 \times 10^{-11} \sqrt{\frac{Y_n(10^{15})}{\tau(ns) R_{HS(\mu m)}}} \left(\frac{T^2}{\sqrt{\langle \sigma v(T) \rangle}} \right) M_f^{-0.2831} \tag{4.9a}$$

$$\beta = 0.2501 \sqrt{\frac{Y_n(10^{15})}{\tau(ns) R_{HS(\mu m)}}} T^{-0.005} M_f^{-0.2831} \tag{4.9b}$$

M_f is the hotspot mass fraction which is given by:

$$M_f = \frac{1.7095 \times 10^{-11}}{M_{DT\,Tot}(\mu g)} \sqrt{\frac{Y_n(10^{15}) R_{HS}^3(\mu m)}{\tau(ns) <\sigma v> (cm^3/sec)}} \tag{4.10a}$$

$$M_f = \frac{8.0602 \times 10^{-3}}{M_{DT\,Tot}(\mu g) T^{2.005}} \sqrt{\frac{Y_n(10^{15}) R_{HS}^3(\mu m)}{\tau(ns)}} \tag{4.10b}$$

The β ignition parameter has been properly normalized so that the probability of ignition should be very high whenever $\beta > 1$.

Springer and Cerjan's original goal was to produce an expression which would infer the hot spot pressure. This is easy to do starting with equation 4.2 for the ion number density. The hot spot pressure is then:

$$P_{HS} = 2 K_B n_{ion} T \tag{4.11}$$

We have assumed that both the electrons and the ions are in thermal equilibrium with the same temperature T. Substitution of equation 4.2 into 4.11 gives us our expression for the hot spot pressure:

$$P_{HS} = 2 K_B \sqrt{\frac{3}{4\pi \chi_D \chi_T}} \sqrt{\frac{Y_n}{\tau R_{HS}^3}} \frac{T}{\sqrt{\langle \sigma v(T) \rangle}} \tag{4.12a}$$

$$P_{HS}(GB) = 3.131 \times 10^{-6} \sqrt{\frac{Y_n(10^{15})}{\tau(ns) R_{HS}^3(\mu m)}} \frac{T}{\sqrt{\langle \sigma v(T) \rangle}} \tag{4.12b}$$

Inserting equation 4.4 into equation 4.12b gives:

$$P_{HS}(GB) = 2.103 \times 10^4 \sqrt{\frac{Y_n(10^{15})}{\tau(ns)R_{HS}^3(\mu m)}} T^{-1.005} \tag{4.12c}$$

Equation 4.12c differs slightly from Springer and Cerjan's results which is reproduced here:

$$P_{HS}(GB) = 2.334 \times 10^4 \sqrt{\frac{Y_n(10^{15})}{\tau(ns)R_{HS}^3(\mu m)}} T^{-1.0} \tag{4.12d}$$

The most likely reason for this small discrepancy is that Springer and Cerjan used a slightly different fit for <σv(T)>. Equation 4.4 represents a least squares fit of the <σv> data used in our ICF codes over the range of 3 to 4.2 KeV. Within the specified temperature range, equation 4.4 will give the closest match to the table lookup data used by our ICF codes.

Again it is trivial to take the hot spot pressure in equation 4.12 and multiply it by the burn duration to get an expression for Pτ.

$$P\tau = 2K_B \sqrt{\frac{3}{4\pi\chi_D\chi_T}} \sqrt{\frac{Y_n\tau}{R_{HS}^3}} \frac{T}{\sqrt{\langle\sigma v(T)\rangle}} \tag{4.13a}$$

$$P\tau(GB \cdot ns) = 3.131 \times 10^{-6} \sqrt{\frac{Y_n(10^{15})\tau(ns)}{R_{HS}^3(\mu m)}} \frac{T}{\sqrt{\langle\sigma v(T)\rangle}} \tag{4.13b}$$

$$P\tau(GB \cdot ns) = 2.103 \times 10^4 \sqrt{\frac{Y_n(10^{15})\tau(ns)}{R_{HS}^3(\mu m)}} T^{-1.005} \tag{4.13c}$$

The expression for Pτ above can be combined with the expression derived in section II for the ignition value of $(P\tau)_{ig}$ found in equation 2.8 to produce an experimentally inferred value for Ricardo Betti's χ.

$$\chi = \frac{P\tau}{(P\tau)_{ig}} = \frac{T_\alpha}{12} \sqrt{\frac{3}{\pi}} \sqrt{\frac{Y_n\tau}{R_{HS}^3}} \left(\frac{\sqrt{\sigma v}}{T}\right) \left[\sqrt{4\chi_D\chi_T}\right] \tag{4.14a}$$

$$\chi = 2.883 \times 10^{11} \sqrt{\frac{Y_n(10^{15})\tau(ns)}{R_{HS}^3(\mu m)}} \left(\frac{\sqrt{\sigma v}}{T}\right) \left[\sqrt{4\chi_D\chi_T}\right] \tag{4.14b}$$

$$\chi = 42.92 \sqrt{\frac{Y_n(10^{15})\tau(ns)}{R_{HS}^3(\mu m)}} T^{1.005} \left[\sqrt{4\chi_D\chi_T}\right] \tag{4.14c}$$

Recall that T_α = 3541 KeV is the energy of the D+T alpha particle. The square root in the square brackets is the correction factor for the DT fuel composition. It reverts to unity in the case of an equimolar mixture. Equation 4.14c has used the power law fit for <σv> found in equation 4.4. Just as in the case of β, χ the probability of ignition should be very high whenever χ > 1.

We can use the same set of approximations to construct a measurement of the η ignition parameter developed in section II as an elaboration of the Larson-Slone ignition figure-of-merit. The definition of the η ignition parameter is given by equation 2.17a – reproduced here with slightly different notation.

$$\eta = \frac{Y_\alpha}{E_{Max}} > 1 \tag{4.15}$$

Y_α is the total energy of all of the 3.5 MeV alpha particles produced in a calculation in which the alpha particles are produced but not allowed to deposit their energy into the DT. E_{max} is the maximum in time of the hotspot thermal energy in a calculation in which the alpha particles are not allowed to deposit any energy into the DT plasma.

It is easy to relate the total alpha yield to the measured neutron yield – Yn:

$$Y_\alpha = Y_n K_B T_\alpha \tag{4.16}$$

Recall that $K_B = 1.60217657 \times 10^{-9}$ is the Boltzmann constant that converts temperature in KeV into energy in ergs. $T_\alpha = 3541$ is the energy of the thermonuclear alpha particle in KeV. The total thermal energy of the hotspot is also easy to express as:

$$E_{max} = \frac{4\pi}{3} R_{HS}^3 \left(2\frac{3}{2} n K_B T\right) \tag{4.17}$$

We can use equation 4.2 to express the average atom density of the hotspot in terms of measured quantities.

$$E_{max} = 4\sqrt{3\pi}\sqrt{\frac{Y_n R_{HS}^3}{\tau\langle\sigma v\rangle}} K_B T \tag{4.18}$$

Now we substitute equations 4.16 and 4.18 back into the definition of η in equation 4.15:

$$\eta = \frac{1}{4\sqrt{3\pi}} \frac{T_\alpha}{T} \sqrt{\frac{Y_n \tau\langle\sigma v\rangle}{R_{HS}^3}} = \frac{T_\alpha}{12}\sqrt{\frac{3}{\pi}}\sqrt{\frac{Y_n \tau}{R_{HS}^3}}\left(\frac{\sqrt{\sigma v}}{T}\right) \tag{4.19}$$

Compare the expression for η in equation 4.19 with the expression for χ found earlier in equation 4.14a. They are in fact identical. This may appear to be a surprise, but it shouldn't. Both χ and η represent that same fundamental assumption – that the hotspot will ignite whenever the Lawson criterion embodied in equation 2.1 is satisfied. Once χ and η are expressed in terms of the same measured quantities Y_n, T, R_{HS} and τ then both ignition parameters reduce to the same

dimensionless expression. This means that Betti's χ and the modified version of Larson and Slone's η are exactly the same when reduced to a measured value.

Finally we give an expression for the Ignition Threshold Factor (experimental) or ITFX which is in common use at Livermore.

$$ITFX = \left(\frac{Y_n}{4.0\times10^{15}}\right)\left(\frac{DSR(\%)}{6.7\%}\right)^{2.1} \tag{4.20}$$

In section V, we will test each ignition parameter and see how well they perform at providing a sharp and unambiguous ignition threshold.

V. The Performance of Ignition Parameters in Simulations of NIF Capsules

In this section we will use detailed one dimensional code simulations of a realistic ignition design to study the performance of 4 ignition parameters. The parameters to be studied are:

1) Ricardo Betti's χ (based on equation 4.14b)
2) Modified Larson-Slone's η (based on equation 4.19)
3) β (based on ρRT^2 in equation 4.9a)
4) ITFX (based on equation 4.20)

Recall that Betti's χ and the modified form of Larson-Slone parameter, η, are identical at the operational level. That is equation 4.14 and 4.19 are identical. So in actuality there are only three ignition parameters to be studied.

The ignition design under consideration in this section uses an ablator made of CH doped with 0.7% silicon. This design was developed as part of a survey on possible ablator materials, but it is very similar to the Revision-5 (Rev-5) design fired many times on NIF.

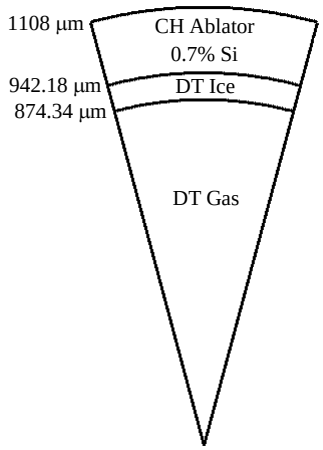

Figure 5.1a: Pie Diagram for B_4C Design

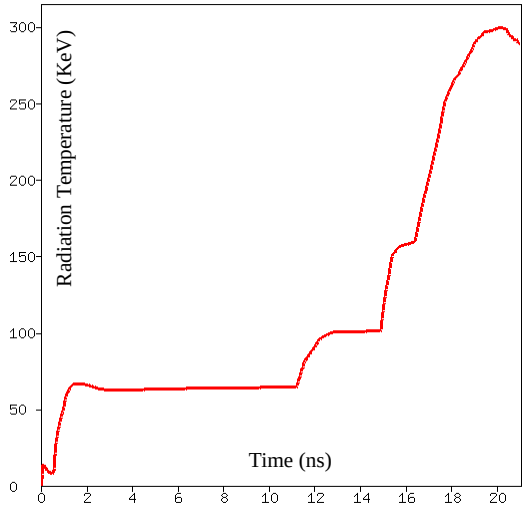

Figure 5.1b: Hohlraum Radiation Temperature for B_4C Design

It is worth mentioning that the Rev-5 or low foot shots on NIF have not ignited and that problem will be taken up in more detail in section VI. However let us comment briefly here that one indication that we have trouble making accurate calculations of Rev-5 is that the measured hotspot pressure inferred from equation 4.12 is always 2 to 5 times lower than the hotspot pressure calculated by our best ICF simulations. There is no guarantee that the CH design used in this section wouldn't suffer from the same type of discrepancy if it were fired on NIF. However we are going to forge ahead with this capsule with the faith that sometime soon, the origin of the

discrepancies between our calculations and the measurements of hotspot conditions will be found and corrected.

Figure 5.1a shows the pie diagram and figure 5.1b shows the equivalent hohlraum radiation temperature for the CH capsule used in this study. It is a conventional four shock ignition design. Figure 5.1b shows the equivalent hohlraum radiation temperature but the actual radiation source was not a pure Planckian.

This NIF design was studied in one dimension with the CALEICF code using the following physics options:

1) Monotonic Sn Radiation Transport
2) Lee-More Electron Thermal Conduction
3) Opacities from the LTE version of the Screen Hydrogenic Model (SHM)
4) Monte-Carlo Charged-Particle Transport
5) Equation of State (EOS) from LEOS Tables (1018 for DT, 5355 for CH)
6) KL Turbulence Mix Model [Dimonte 2006]

In all calculations the energy deposition of the thermonuclear neutrons was completely neglected which is a reasonable approximation for a NIF scale capsule. In some of the simulations the thermonuclear alpha particles properly deposited their energy back into the plasma. Such simulations are known as full burn or alpha-on calculations. In other simulations the thermonuclear neutron and alpha particles will be produced and counted but no alpha energy will be deposited back into the plasma. Such simulations will be known as no-alpha or alpha-off simulations. When simulated with a clean (no KL mix) calculation, the capsule depicted in figure 5.1 absorbs 154.6 KJ and produces a yield of 20.7 MJ.

Clean one dimensional simulations provide only a limited guide to the actual performance of this or any ICF capsule. Real ICF capsules simply do not implode and burn like clean one dimensional calculations. Obviously the most reliable computational model would be numerically converged, three dimensional simulations but no one has succeeded in performing a single such converged calculation, let alone the hundreds of calculations needed in this study. As a consequence, we will take a less accurate but more practical approach of introducing an empirical mix model into our one dimensional simulations.

The KL turbulent mix model was developed to reproduce the observed Rayleigh-Taylor and Richtmyer-Meshkov mixing measured by the Linear Electric Motor (LEM) experiments [Dimonte 1996, Dimonte 2006]. By its construction the KL model should do reasonably well in representing the Rayleigh-Taylor and Richtmyer-Meshkov mixing experienced at the fuel-ablator interface. The KL model also predicts significant mixing at the hot-spot/cold-fuel

boundary as well as at the ablation front. Detailed two and three dimensional simulations also predict significant mixing in all three of these regions. However close comparison of the two and three dimensional results with the KL results in one dimension reveal that the KL model is qualitatively correct but not always quantitatively correct in all details. However in spite of this flaw, one dimension simulations of ICF capsules with the KL model are much more realistic than clean calculations.

In a KL simulation the initial roughness of a capsule surface can be represented by the initial value of the L field at the surface in question. The square root of the sum of the squares of the amplitudes for all modes greater than 50 is about 200nm for the inner DT ice of a typical NIF shot. When the same procedure is done for the inner surface of a plastic ablator the result is a surface roughness of about 10nm. The comparable value for the outer surface of a plastic ablator is around 50nm. These values set the scale for the initial L field at these three critical surfaces for a standard Rev-5 plastic ablator capsule fired on NIF. However when these nominal values of initial L are used in one dimensional KL calculations of real NIF shots, the calculated yields are almost always higher than the measured ones. The exception to this over-optimistic behavior are some of the recent high foot shots in which KL simulations initialized with the nominal values for the surface roughness come close to matching the observed data.

This problem of overly optimistic calculated yields is not limited to the KL model. Highly resolved two and three dimensional calculations of actual NIF shots nearly always over predict the measured yields as well. A common fudge around this problem is to arbitrarily increase the initial surface roughness of the outer ablator. Few researchers believe this is an accurate model of reality, instead it is seen as a convenient way to degrade the yield of the calculation until it matches the measured value. In much the same way, one dimensional KL calculations can be forced to match experimental yields by arbitrarily increasing the initial surface roughness of the L field on all three surfaces until the calculated yield matches the observed value. An initial L value of around 1000nm placed on all three surfaces generally comes close to matching the observed NIF yields of the low foot Rev-5 shots.

This trick of increasing the initial value of L in order to degrade the calculated performance of a capsule is exploited in this section to explore the various ignition criteria. Two different series of calculations were done with the CH capsule described in figure 5.1. In the first series, the initial value of L was 200nm. This initial L value was used at the inner DT ice surface, the ice/ablator interface and at the outer ablator surface. The radiation drive for the capsule was randomly varied about the nominal drive depicted in figure 5.1b. The temperatures of the foot along with the temperatures of the second, third and main pulses were randomly varied both up and down.

For each variation of the radiation drive, two calculations were performed using that same drive. In the first calculation, the thermonuclear reactions were turned on but the alpha energy

depositions were disabled. The neutron yield, Yn, the temperature, T, determined by the neutron-time-of-flight spreading, the hotspot radius, R_{HS}, determined by the neutron pinhole image, the burn time, τ, determined by the full-width half-max of the thermonuclear gamma signal and the down scattered ratio (DSR) were all extracted from the no-alpha calculation exactly as if the no-alpha calculation was a synthetic experiment. These five synthetic measurements were inserted into equations 4.9b and 4.10b to determine the measured value of β which is based upon ρRT^2. They were also inserted into equation 4.14b to determine Betti's χ (which is identical to modified Larson-Slone η). Lastly these synthetic measurements were inserted in equation 4.20 to determine the measured value of ITFX.

In the second calculation for a given drive variation the alpha energy depositions were turned on and the specific yield was recorded. The blue diamonds in figures 5.2, 5.3 and 5.4 present the results of the first series with an initial L value of 200nm. The specific yield is the total yield of the capsule divided by the initial DT mass of the capsule. The specific yield is plotted in units of megajoules per milligram. Note that if all of the deuterium and tritium in an equimolar mixture are consumed by the D+T reaction the specific yield would be 337.4 MJ/mg.

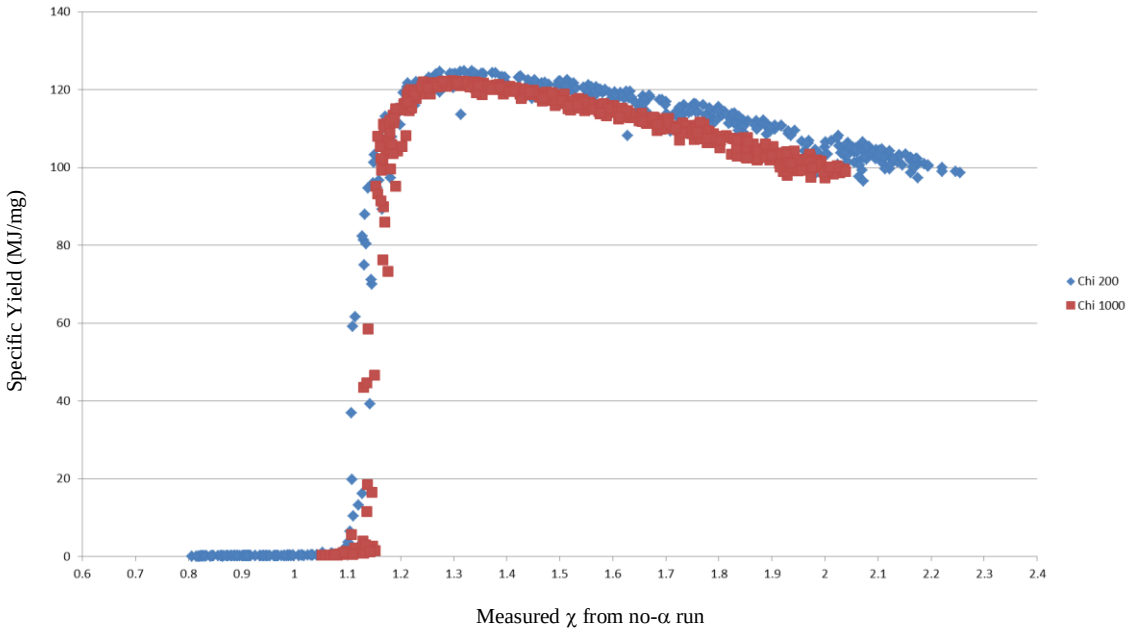

Figure 5.3: Specific yields vs. χ for 500 random variations of the drive for the CH ignition capsule described in figure 5.1. The blue diamond series represent calculations in which all surfaces were initialized with an L value of 200nm. The red square series represent calculations initialized with an L value of 1000nm.

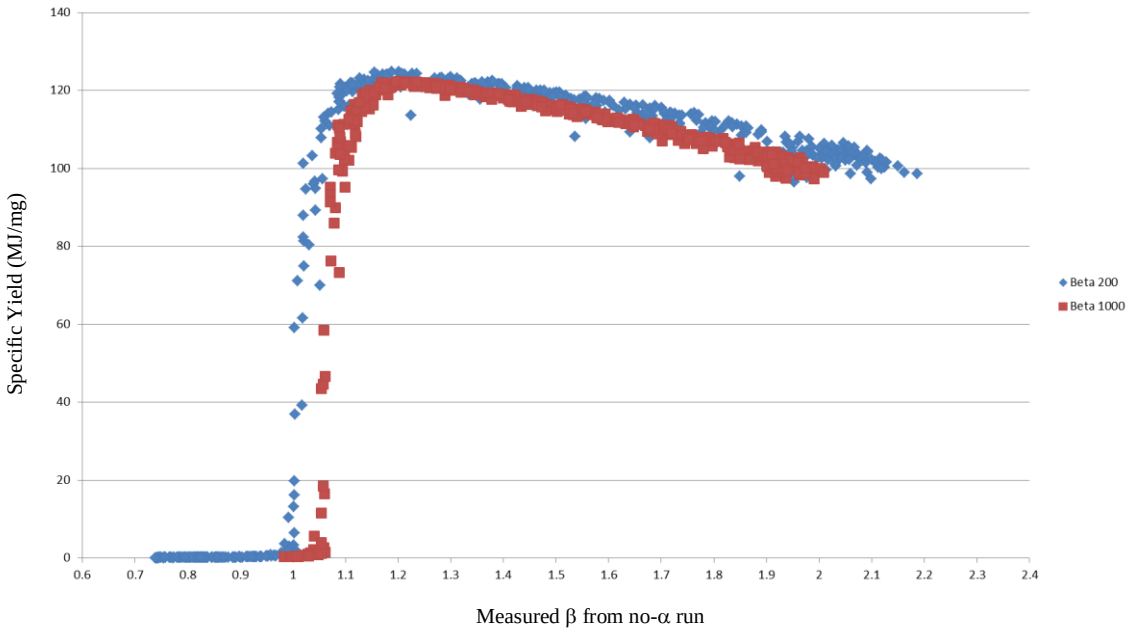

Figure 5.4: Specific yields vs. β (based on ρRT^2) for 500 random variations of the drive for the CH ignition capsule described in figure 5.1. The blue diamond series represent calculations in which all surfaces were initialized with an L value of 200nm. The red square series represent calculations initialized with an L value of 1000nm.

A second series of random drive variations were performed with the initial L value of 1000nm on all three capsule surfaces. The random drive variations of this second series were similar but not identical to the drive variations used in the first series described above. In all other respects the second series was identical to the first. The red squares in figures 5.2, 5.3 and 5.4 present the results of the second series with an initial L value of 1000nm.

Notice that all three ignition parameters perform well in the task of sorting failed drive variations from igniting drive variations. Even as the degradations due to the mix model are increased by increasing the initial L from 200nm to 1000nm the location of the ignition cliff barely moves.

This is the characteristic of a good ignition parameter. Let us imagine for a moment a typical calculation near the ignition cliff. If we increase the mix by increasing the initial L, then the specific yield should drop and we would expect the location of the ignition surface to move to the right in the direction of larger values of the ignition parameter. However, the increase in mix also decreases the calculated value of the ignition parameter and the location of the calculated point moves both downward and to the left. This behavior applies to all points near the ignition cliff. With increased mix, they all move downward and to the left, leaving the location of the ignition cliff largely unchanged.

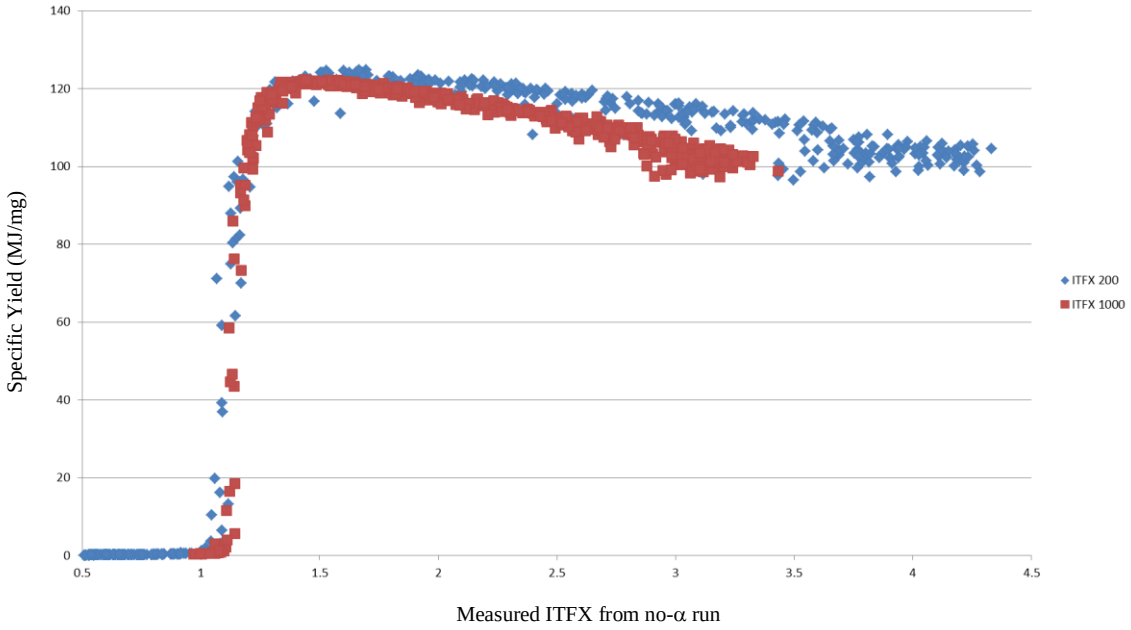

Figure 5.5: Specific yields vs. ITFX for 500 random variations of the drive for the CH ignition capsule described in figure 5.1. The blue diamond series represent calculations in which all surfaces were initialized with an L value of 200nm. The red square series represent calculations initialized with an L value of 1000nm.

Brian Spears has recommended an alternative way to graphically display the ignition cliff for a given ignition parameter. These are presented in figures 5.6, 5.7 and 5.8. In each of these figures, the vertical axis is the ratio of the full burn yield divided by the no-alpha yield. The horizontal axis is once again the ignition parameter inferred from the no-alpha calculations. Brian observed that the peak of such plots occurs near the top of the ignition cliff and are sharply defined and for this reason they provide a clear marker for the location of the ignition cliff.

Figure 5.6 plots the yield ratio verses the measured values of χ. The peak yield ratio for the series with an initial L of 200nm occurs at $\chi = 1.21$. The peak yield ratio for the series with an initial L of 1000nm occurs at $\chi = 1.20$. This is very consistent behavior and is the attribute of a good ignition parameter. It should be noted that there is no numerical normalization to χ. The ignition criterion of $\chi > 1$ is nothing more than a consistent application of Lawson's original hypothesis. The fact that the capsule studied in this section exhibits a threshold near $\chi = 1.2$ confirms the validity of Lawson's hypothesis.

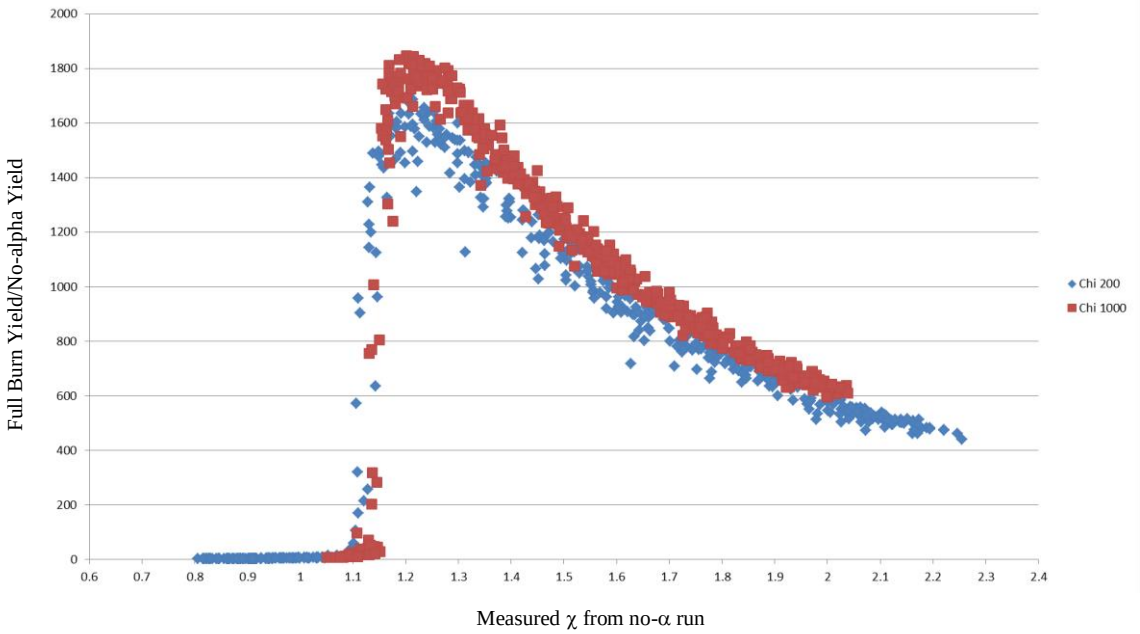

Figure 5.6: The ratio of the full burn yield to the no-alpha yield vs. the experimentally inferred value of χ. The blue diamond series represent calculations in which all surfaces were initialized with an L value of 200nm. The red square series represent calculations initialized with an L value of 1000nm. The peak of the yield ratio is a good marker for the location of the ignition cliff. For the L = 200nm series the peak occurs at χ = 1.21. For the L = 1000 nm series the peak occurs at χ = 1.20.

Figure 5.7 plots the yield ratio verses the measured values of β based on ρRT^2. The peak ratio for the L0 = 200nm series is at β = 1.09 and the peak ratio for the L0 = 1000nm series occurs at β = 1.11. Once again this is very consistent behavior and indicates that β is a good ignition parameter. Unlike the case of χ, the fact that the ignition threshold for β is near unity should not be a surprise because the definition of β includes a normalization factor derived from solving the tamped Meldner problem so β has already been normalized by numerical calculations.

Figure 5.8 plots the yield ratio verses the measure values of ITFX. The peak ratio for the L0 = 200nm series is ITFX = 1.21. The peak ratio for the L0 = 1000nm series is ITFX = 1.34. Once again we see consistent behavior which indicates that ITFX is a good ignition parameter. However the fact that the ignition threshold for ITFX is near 1.25 is a bit of a surprise. The original intent behind ITFX was to normalize it such that an ITFX value of 1.0 would represent a 50% chance of ignition. Look closely at figure 5.5 again. The midpoint of the ignition cliff is around ITFX = 1.15 rather than the expected 1.00. I'm not sure what caused this discrepancy.

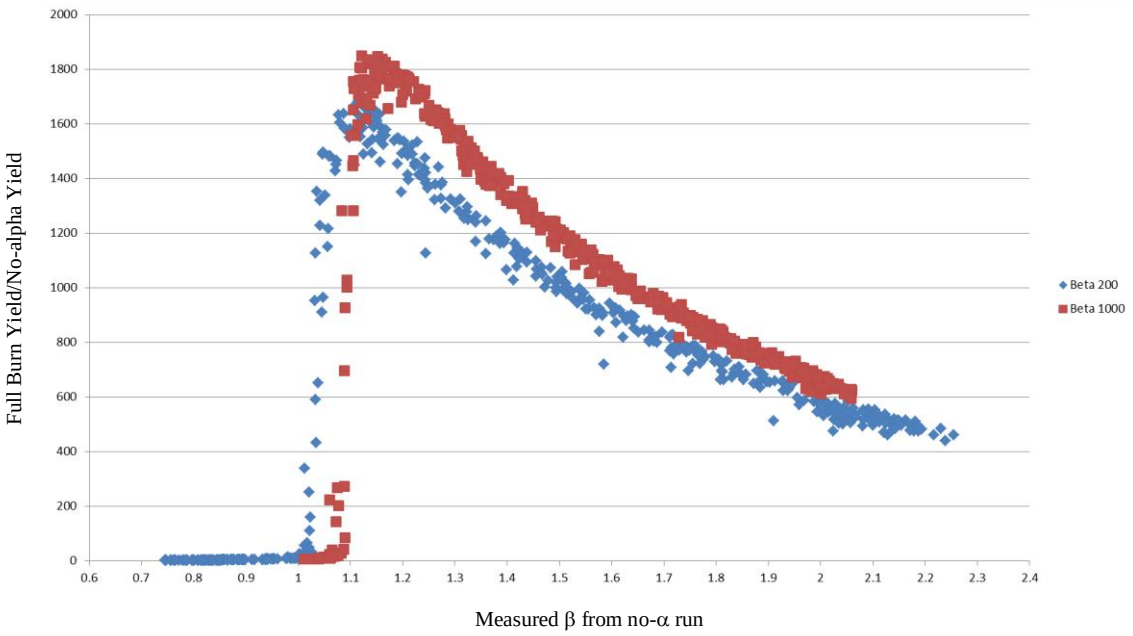

Figure 5.7: The ratio of the full burn yield to the no-alpha yield vs. the experimentally inferred value of β. The blue diamond series represent calculations in which all surfaces were initialized with an L value of 200nm. The red square series represent calculations initialized with an L value of 1000nm. The peak of the yield ratio is a good marker for the location of the ignition cliff. For the L = 200nm series the peak occurs at β = 1.09. For the L = 1000 nm series the peak also occurs at β = 1.11.

Figure 5.9 explores the relationship between χ and ITFX by plotting the measured ITFX from the no-alpha calculations verses the measured χ also from the no-alpha calculations. Also plotted is the least squares fit to a power law which turns out to be:

$$ITFX = 0.80084\chi^{2.1765} \tag{5.1}$$

According to Brian Spears the expected relationship between ITFX and χ should be:

$$ITFX = \chi^{8/3} = \chi^{2.6667} \tag{5.2}$$

Since χ exhibits an ignition threshold near χ = 1.20, if equation 5.2 was true then we would expect ITFX to exhibit an ignition threshold near:

$$ITFX(Theshold) = (1.20)^{8/3} = 1.62 \tag{5.3}$$

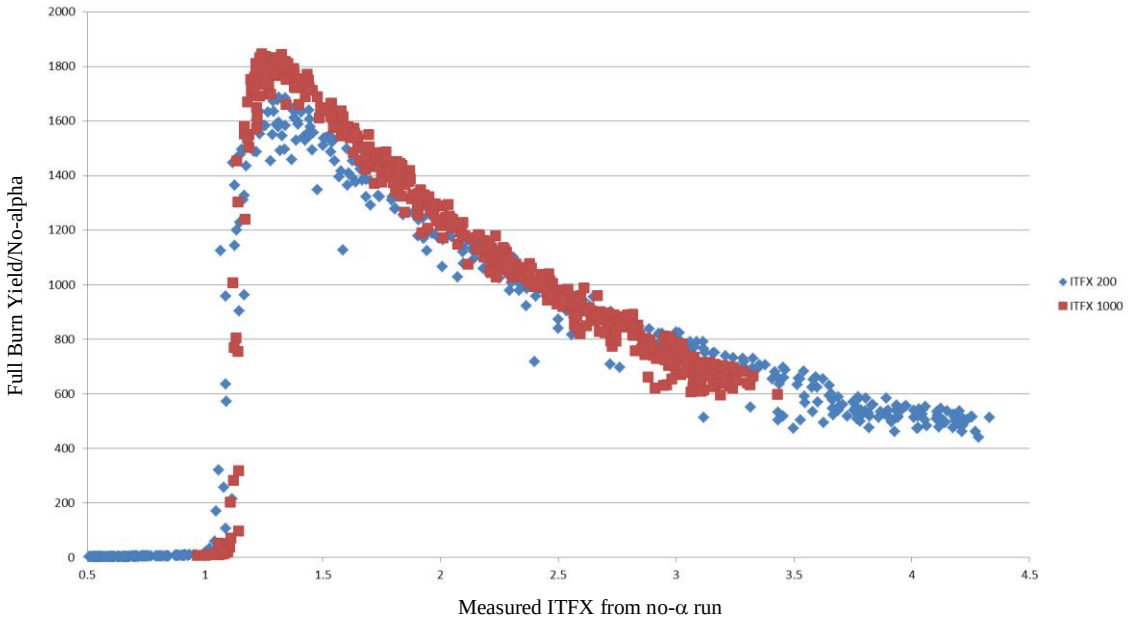

Figure 5.8: The ratio of the full burn yield to the no-alpha yield vs. the experimentally inferred value of ITFX. The blue diamond series represent calculations in which all surfaces were initialized with an L value of 200nm. The red square series represent calculations initialized with an L value of 1000nm. The peak of the yield ratio is a good marker for the location of the ignition cliff. For the L = 200nm series the peak occurs at ITFX = 1.31. For the L = 1000 nm series the peak occurs at ITFX = 1.24.

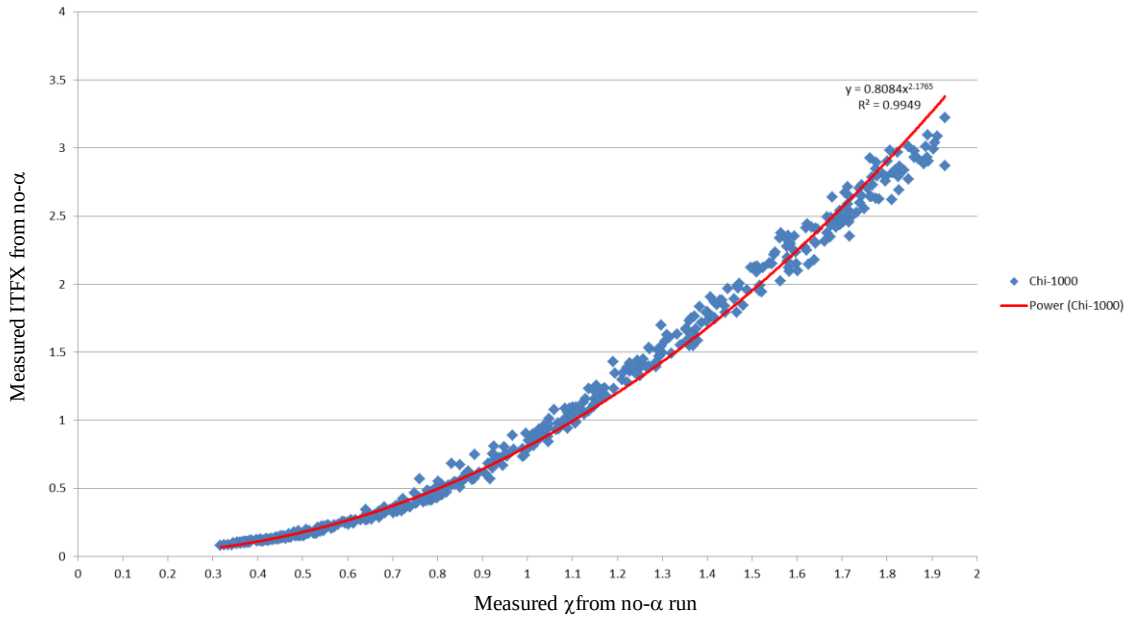

Figure 5.9: The measured ITFX vs. the measured χ. Both ignition parameters were taken from no-alpha runs. Also plotted is the least squares fit to a power law which is ITFX = 0.8084 $\chi^{2.1765}$.

However figure 5.9 demonstrates that equation 5.2 is not true of the numerical simulations. The observed relationship between ITFX and χ is summarized by equation 5.1. Hence we expect ITFX to exhibit a threshold near:

$$ITFX(Theshold) = 0.8084(1.20)^{2.1765} = 1.20 \qquad (5.4)$$

Figure 5.8 shows that ITFX does in fact exhibit an ignition threshold very close to ITFX = 1.2.

In the real world it is not possible to turn off alpha energy depositions and yet the ignition thresholds are conventionally formulated in terms of no-alpha ignition parameters. It is useful to discovery a relation between the ignition parameters with alpha depositions turned on and the ignition parameters with alpha depositions turned off. Figures 5.10, 5.11 and 5.12 plot the ignition parameters with alpha depositions turned off in the vertical versus alpha depositions turned on along the horizontal. The data points were taken from the L0 = 1000nm series discussed earlier in this section. The figures also plot simple fits to the data shown as the red curves.

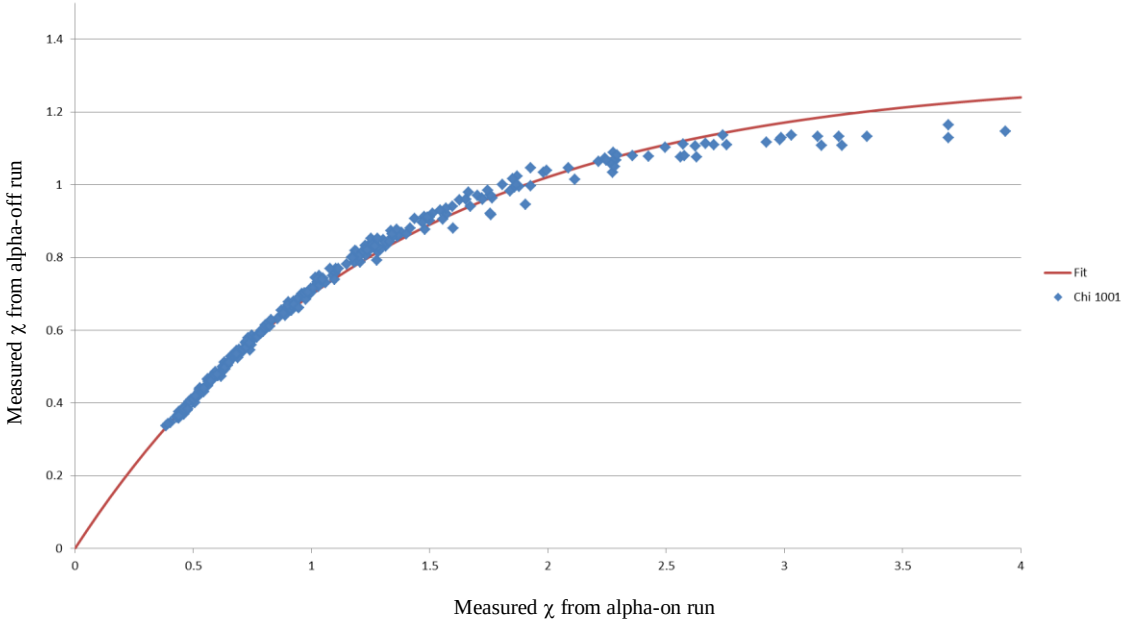

Figure 5.10: The measured χ from alpha-off calculation vs. the measured χ from alpha-on calculation. The red curve is a simple fit (equation 5.5).

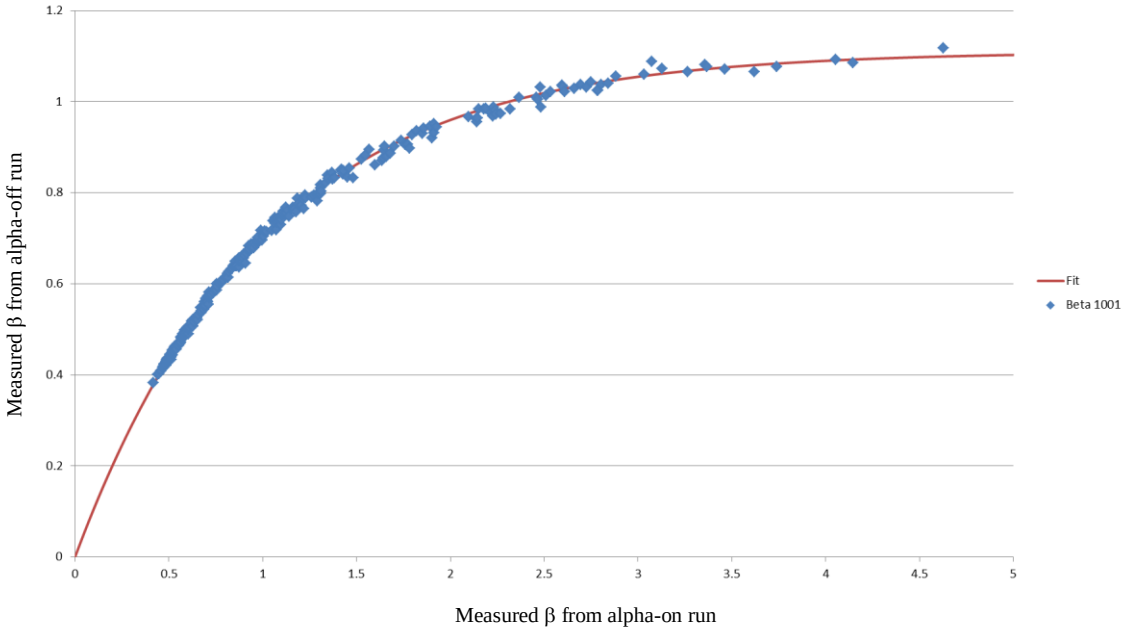

Figure 5.11: The measured β from alpha-off calculation vs. the measured β from alpha-on calculation. The red curve is a simple fit (equation 5.6).

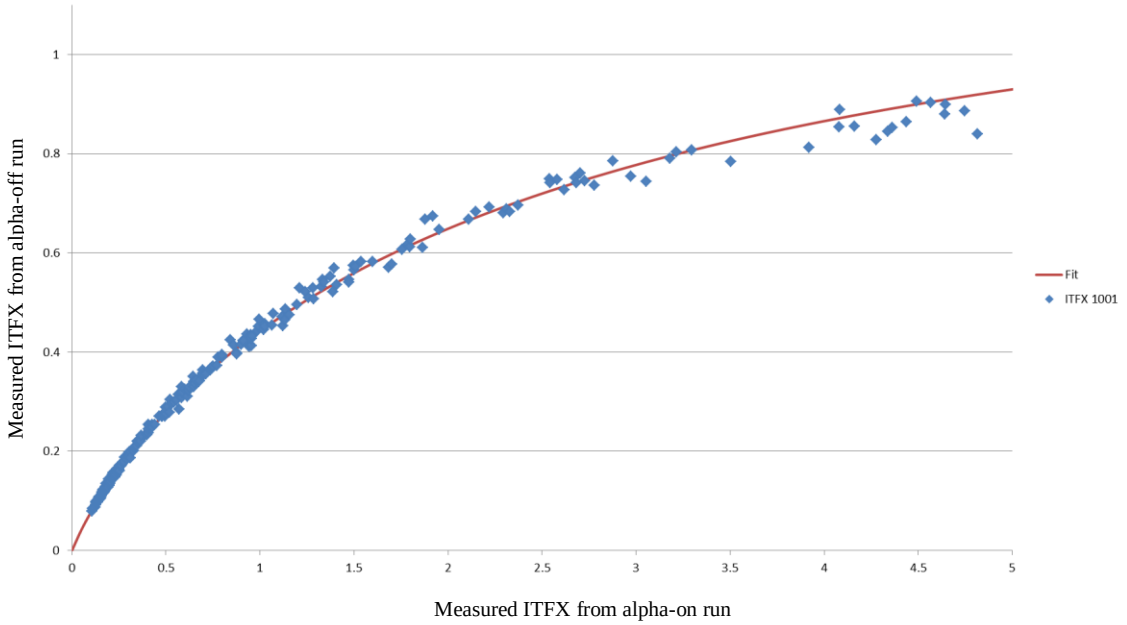

Figure 5.12: The measured ITFX from alpha-off calculation vs. the measured ITFX from alpha-on calculation. The red curve is a simple fit (equation 5.7).

Simple fits were found for all three data patterns. For the ignition parameter χ, the best fit was:

$$\chi_{\alpha-Off} = 1.3\left(1 - exp(-0.77\chi_{\alpha-On})\right) \tag{5.5}$$

The RMS error for the χ fit is 2.5%. For the ignition parameter β, the best fit was:

$$\beta_{\alpha-Off} = 1.11\left(1 - exp(-\beta_{\alpha-On})\right) \tag{5.6}$$

The RMS error for the β fit is 1.2%. For ITFX, the best fit was:

$$ITFX_{\alpha-Off} = \left[1.11\left(1 - exp\left(-0.90909(ITFX_{\alpha-On})^{1/1.94}\right)\right)\right]^{1.94} \tag{5.7}$$

The RMS error for the ITFX fit is 2.7%.

In section VI, we will use these fits to transform measured alpha-on data from NIF shots into the expected alpha-off values.

VI. Ignition Parameters on NIF shots

We can use the expressions developed in section IV to infer the experiment values of ρRT^2, β, χ and ITFX for a collection of actual NIF shots. Table 6.1 presents some of the basic data for 25 NIF shots. The average ion temperature (Tion) was determined by the time of flight spreading to the NTOF detector. The burn duration (τ) was taken as the FWHM of the thermonuclear gamma signal. The radius of the hot spot (R_{HS}) was taken from the P_0 moment of the 17% contour from the neutron pin-hole image. The down scattered ratio (DSR) is the ratio of measured number of neutrons between 10 to 12 MeV divided by the measured number of neutrons between 13 and 15 MeV.

Table 6.1 Measured Data from 25 NIF Shots

Shot	Yn	Tion	τ	R_{HS}	DSR
	10^{15}	KeV	ns	μm	%
110603	0.0642616	2.63884	0.220	25.3	4.326
110608	0.190962	3.10552	0.215	33.0	4.333
110615	0.43002	3.31903	0.215	38.4	3.537
110620	0.4113	4.3157	0.122	24.5	4.526
110826	0.17054	3.0617	0.180	25.0	3.880
110914	0.574	3.58679	0.171	28.3	4.880
111103	0.231342	3.2844	0.190	30.1	3.914
111112	0.602045	3.89828	0.154	30.9	4.211
111215	0.745	3.5325	0.180	28.0	4.307
120126	0.317184	2.87943	0.175	24.9	3.917
120131	0.620336	3.87902	0.199	32.7	3.698
120205	0.604543	3.43133	0.155	28.0	4.347
120321	0.415645	3.06822	0.158	26.0	6.258
130501	0.767	3.02	0.172	37.9	2.960
130802	0.48	2.85	0.216	38.9	2.840
130927	4.42	4.43	0.188	35.4	3.660
131119	5.237	4.77	0.156	37.2	3.800
140120	8.002	5.58	0.170	35.2	3.900
140304	8.125	5.83	0.168	33.9	3.820
140511	6.1813	5.36	0.147	33.2	4.040
140520	5.237	5.49	0.156	37.2	4.320
141123	1.100	3.40	0.108	25.7	5.450
131212	1.830	3.55	0.161	33.0	2.300
140722	0.371	3.38	0.198	38.9	2.080
140926	0.280	3.84	0.154	36.6	2.200

The experimental numbers listed in table 6.1 were inserted into equations 4.7b, 4.8b and 4.9b to determine the β ignition parameter based on ρRT^2. They were also inserted into equation 4.14b to determine the χ ignition parameter and finally they were inserted into equation 4.20 to determine ITFX. The inferred ignition parameters for the 25 NIF shots are listed in table 6.2.

Table 6.2: Inferred Ignition Parameters

Shot	Yn	Spec Y	β	χ	ITFX
	10^{15}	MJ/mg	---	---	---
110603	0.0642616	0.001034	0.1582	0.1025	0.0064
110608	0.190962	0.003011	0.1433	0.1413	0.0191
110615	0.43002	0.007253	0.1689	0.1815	0.0281
110620	0.4113	0.006819	0.3613	0.3386	0.0451
110826	0.17054	0.002804	0.1856	0.1826	0.0135
110914	0.574	0.009318	0.2842	0.3204	0.0738
111103	0.231342	0.003767	0.1776	0.1783	0.0187
111112	0.602045	0.009677	0.2917	0.2965	0.0568
111215	0.745	0.011971	0.3083	0.3745	0.0736
120126	0.317184	0.005258	0.2280	0.2304	0.0257
120131	0.620336	0.010266	0.2519	0.3119	0.0445
120205	0.604543	0.010070	0.2933	0.3042	0.0609
120321	0.415645	0.006581	0.2614	0.2523	0.0900
130501	0.767	0.012599	0.2190	0.1997	0.0334
130802	0.48	0.007867	0.1621	0.1592	0.0198
130927	4.42	0.068884	0.5349	0.8118	0.3104
131119	5.237	0.081617	0.6103	0.7946	0.3979
140120	8.002	0.128041	0.8075	1.2603	0.6421
140304	8.125	0.129543	0.8736	1.3759	0.6242
140511	6.1813	0.098553	0.7933	1.0889	0.5342
140520	5.237	0.083498	0.6707	0.8859	0.5209
141123	1.100	0.018234	0.3773	0.4845	0.1782
131212	1.830	0.030521	0.3681	0.4494	0.0484
140722	0.371	0.006079	0.1744	0.1504	0.0080
140926	2.800	0.047319	0.4059	0.5145	0.0675

A close inspection of table 6.2 reveals that some of the recent high foot shots have come very close to the expected ignition threshold. Take for example shot N140304. It has an inferred value of β = 0.8736 and an inferred value of χ = 1.3759. We saw in section V, that the ignition threshold for β with no alpha depositions was β = 1.1 (see figure 5.7). The threshold for χ with no alpha depositions was around χ = 1.2 (see figure 5.6). Shot N140120 also appears to be near the expected threshold with an inferred β of 0.8075 and an inferred χ of 1.2603.

Based on their measured values for β and χ, both N140120 and N140304 appear to be very close to the ignition threshold but unfortunately that appearance is somewhat misleading. These high performing shots almost certainly experienced significant alpha heating and the measured values of β or χ no longer correspond to the no-alpha values used to estimate the location of the ignition thresholds in section V. The effect of alpha heating increases the measured values of β and χ and therefore gives the appearance that the shot is closer to the ignition threshold than is warranted. However the observation that the best performing shots have experienced significant alpha heating is in itself, evidence that these shots are getting close to ignition.

In section V we noted correlations between ignition parameters with alpha depositions turned on and alpha depositions turned off. These correlations are reproduced here:

$$\beta_{\alpha-Off} = 1.11\left(1 - exp(-\beta_{\alpha-On})\right) \tag{5.6}$$

$$\chi_{\alpha-Off} = 1.3\left(1 - exp(-0.77\chi_{\alpha-On})\right) \tag{5.5}$$

$$ITFX_{\alpha-Off} = \left[1.1\left(1 - exp\left(-0.90909(ITFX_{\alpha-On})^{1/1.94}\right)\right)\right]^{1.94} \tag{5.7}$$

These correlations fit the data of section V with errors of 1 to 3%. We can use these correlations to transform the measured ignition parameters with alpha depositions turned on listed in table 6.2 into the equivalent values we would expect if we could turn off alpha depositions in nature. Table 6.3 lists the transformed ignition parameters for the 25 NIF shots.

Notice that the transformed ignition parameters of the best performing shots such as N140120 and N140304 are still very high but have dropped below the expected ignition thresholds.

Figures 6.1, 6.2 and 6.3 compare the NIF data for each ignition parameter against the L0 = 1000nm series of calculations described in section V. In each figure the horizontal axis is the ignition parameter and the vertical axis is the specific yield in MJ/mg. The horizontal axis for the blue squares use the calculated ignition parameter with alpha depositions turned on. The horizontal axis for the red squares use the calculated ignition parameter with alpha depositions turned off. The horizontal axis for the green triangles use the inferred ignition parameters for the NIF listed in table 6.2 (alpha-on values). The horizontal axis for the purple triangles use the transformed ignition parameters listed in table 6.3 (alpha-off values).

Table 6.3: Expected No-Alpha Ignition Parameters			
Shot	β	χ	ITFX
	---	---	---
110603	0.1625	0.0987	0.0060
110608	0.1482	0.1340	0.0171
110615	0.1725	0.1696	0.0245
110620	0.3366	0.2984	0.0378
110826	0.1881	0.1705	0.0123
110914	0.2746	0.2842	0.0589
111103	0.1806	0.1668	0.0167
111112	0.2808	0.2654	0.0466
111215	0.2945	0.3257	0.0588
120126	0.2263	0.2113	0.0225
120131	0.2471	0.2776	0.0374
120205	0.2822	0.2715	0.0496
120321	0.2553	0.2295	0.0702
130501	0.2183	0.1853	0.0296
130802	0.1661	0.1500	0.0176
130927	0.4598	0.6042	0.1955
131119	0.5070	0.5949	0.2360
140120	0.6150	0.8074	0.3320
140304	0.6466	0.8494	0.3256
140511	0.6079	0.7379	0.2922
140520	0.5424	0.6428	0.2870
141123	0.3488	0.4048	0.1255
131212	0.3418	0.3803	0.0404
140722	0.1777	0.1422	0.0074
140926	0.3704	0.4252	0.0544

Notice in figures 6.1 and 6.2 both the red and the blue calculated series seem to converge near $\beta = \chi = 0.4$ and both series appear to pass through the cluster of low performing NIF shots. It would appear that there is not much alpha heating below $\beta = \chi = 0.4$. However a closer examination of figures 6.1 and 6.2 reveals that even below 0.4, the presence of alpha heating can shift the β or χ coordinate by 20% or more. Only when β or χ drops below 0.2 do the alpha-on and the alpha-off coordinates differ by less than 10%.

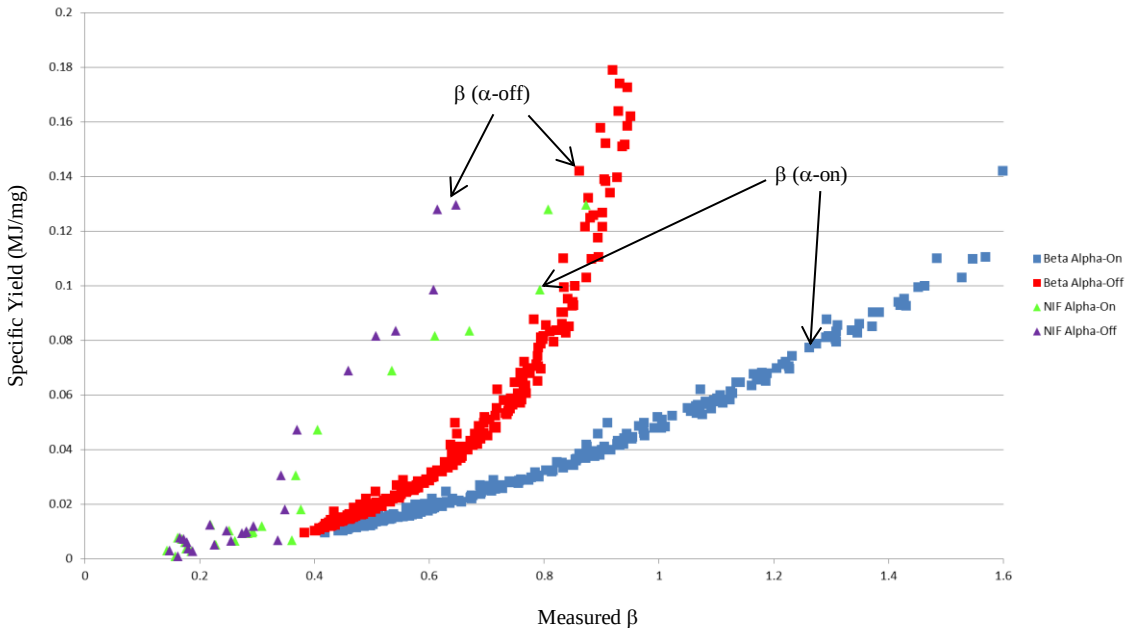

Figure 6.1: The specific yield versus the inferred ignition parameter β. The triangles represent NIF data. The squares came from the L0 = 1000nm series of section V. The blue squares include alpha energy depositions. The red squares omit alpha depositions. The green triangles represent measured NIF data. The β values of the purple triangles have been transformed into no-alpha equivalent by equation 5.6.

The separation of the alpha-on and alpha-off data series is a little easier to see in figure 6.3 which uses ITFX as the horizontal coordinate. The red series (alpha-off) terminates around ITFX = 0.08 while the blue series (alpha-on) terminates around ITFX = 0.12. This means that even with ITFX as low as 0.10, the effect of alpha heating can change the ITFX parameter by more than 50%.

Notice in figure 6.1 using β as the coordinate, the NIF data points are quite a bit higher than the calculated points. Having the measured specific yields higher than the calculated yields sounds like a good thing, but such behavior casts doubt on the value of the calculated series as a guide for the likely performance of future shots.

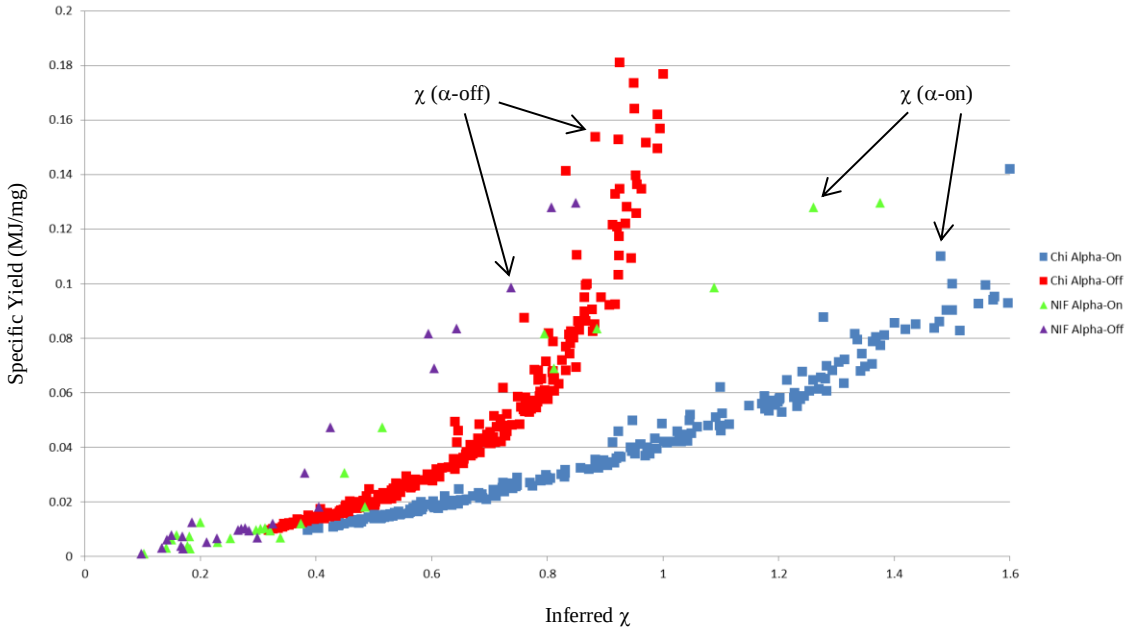

Figure 6.2: The specific yield versus the inferred ignition parameter χ. The triangles represent NIF data. The squares came from the L0 = 1000nm series of section V. The blue squares include alpha energy depositions. The red squares omit alpha depositions. The green triangles represent measured NIF data. The χ values of the purple triangles have been transformed into no-alpha equivalent by equation 5.5.

The situation is better in figure 6.2 which uses χ as the coordinate. Here we see rough agreement between the NIF data points and the calculated series. There is rough agreement for the actual NIF points which have alpha depositions turned on but there is also rough agreement for the transformed NIF points which represent what would happen if we could turn off the alpha depositions in the experiment.

Figure 6.3 using ITFX as the horizontal coordinate agrees with the data about as well as the β parameter seen in figure 6.1. There is a good chance that if the calculated series were continued to lower levels of performance, the general trend of the calculated series would pass right through the cluster of low performing NIF shots. However the high performing NIF shots do not match the calculated series very well. It doesn't really matter whether we consider curves with alpha depositions on or off. Either way the high performing shots don't match the calculated trends.

Overall, the ignition parameter that produces the best match to the data is χ, plotted in figure 6.2. The agreement is by no means perfect, but the calculated and measured points are following similar trends. This is true for both the alpha-on plots as well as the alpha-off plots.

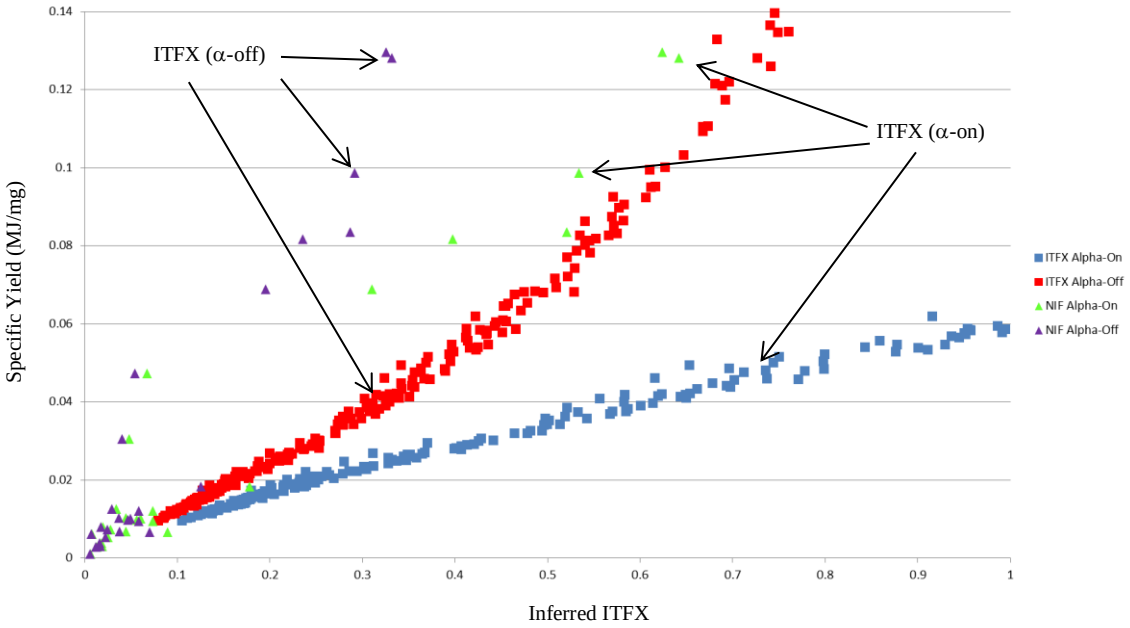

Figure 6.3: The specific yield versus the inferred ignition parameter ITFX. The triangles represent NIF data. The squares came from the L0 = 1000nm series of section V. The blue squares include alpha energy depositions. The red squares omit alpha depositions. The green triangles represent measured NIF data. The ITFX values of the purple triangles have been transformed into no-alpha equivalent by equation 5.7.

Figure 6.4 is the same as figure 6.2 with the vertical axis extended to higher specific yields. This allows us to see just how close the best NIF shots are to climbing up the steepest part of the ignition cliff represented by the calculational series plotted with the red squares. If the calculations bear any resemblance to reality, then even small increases in hotspot pressure should result in much larger increases in neutron yield.

The best shots have an estimated χ(alpha-off) of 0.85. Ignition should occur with an χ(alpha-off) of around 1.2. This means if the hotspot pressure could be increased by 50% while leaving the time τ and the temperature T unchanged, it is very likely NIF would finally achieve ignition.

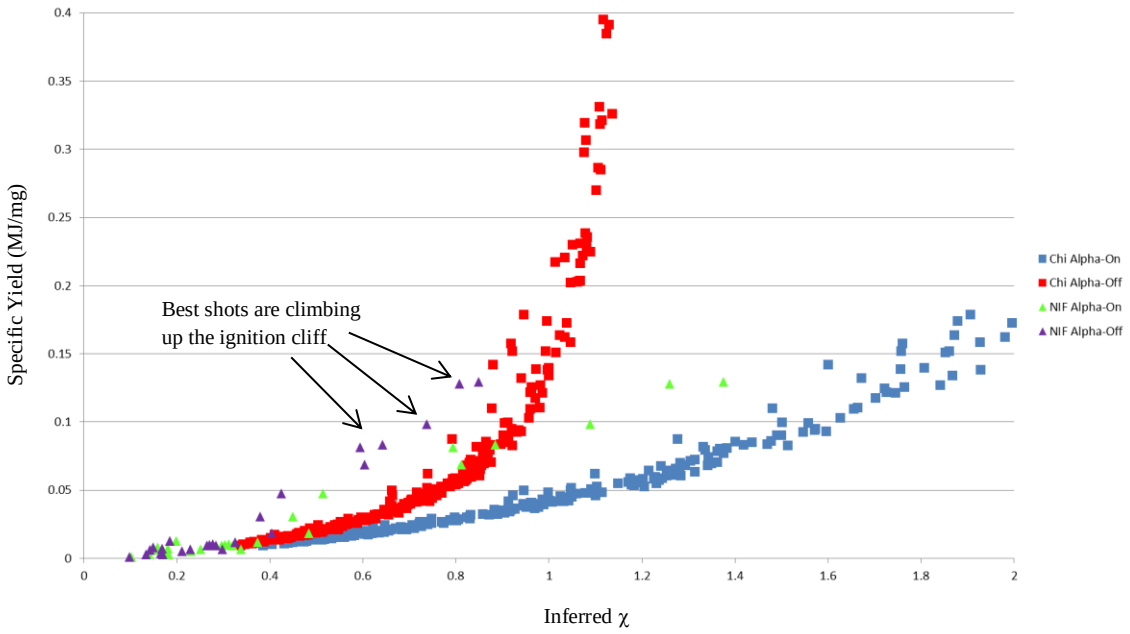

Figure 6.4: The specific yield versus the inferred ignition parameter χ. The triangles represent NIF data. The squares came from the L0 = 1000nm series of section V. The blue squares include alpha energy depositions. The red squares omit alpha depositions. The green triangles represent measured NIF data. The χ values of the purple triangles have been transformed into no-alpha equivalent by equation 5.7. The best shots are climbing up the ignition cliff.

However there is a well-known discrepancy between the hotspot pressure estimated by ICF codes and the measured hotspot pressured inferred from equation 4.12. Table 6.4 lists the experimentally inferred hotspot pressures and the code calculation of the hotspot pressures. Note that the actual pressures are 20% to 80% of the code's calculated pressures. If the source of this discrepancy could be found and corrected in some way, the resulting increase in hotspot pressure would most likely increase all ignition parameters to the point that ignition would follow.

Table 6.4: Measured and Predicted Hotspot Pressures			
Shot	Measured P	Code P	Measured/Code
	Gbars	Gbars	---
110603	34.58	152.27	0.2271
110608	33.58	147.52	0.2276
110615	37.37	89.78	0.4162
110620	73.78	181.43	0.4066
110826	53.40	258.36	0.2067
110914	70.60	262.23	0.2692
111103	42.45	144.94	0.2929
111215	80.93	209.84	0.3857
120126	79.66	145.98	0.5457
120131	50.69	142.85	0.3549
120205	80.87	115.00	0.7032
120321	83.71	186.58	0.4486
130501	62.91	72.13	0.8722
130802	45.63	137.58	0.3317
130927	109.28	207.25	0.5273
140120	129.55	344.57	0.3760

VII. Conclusions

In this report, four ignition parameters have been studied, χ, β, η, and ITFX. In section II all of the associated ignition criteria except for ITFX were derived from Lawson's fundamental hypothesis that ignition occurs when the thermonuclear heating rate exceeds the plasma's cooling rate or dissipation rate. It has been shown elsewhere and confirmed in section V that ITFX is highly correlated with the χ ignition parameter and hence all of the other Lawson based ignition parameters. Also in section V, it was shown that all four of the ignition parameters studied perform well on realistic one-dimensional calculations of a NIF ignition design. Hence one conclusion of this report is that even though these ignition parameters differ in some of their details, their theoretic underpinning and their actual performance as ignition parameters are all very similar.

In section IV it shown that all of the ignition parameters could be inferred directly from the NIF data with minimal reliance on ICF codes. In section VI the measured performance of 25 NIF shots was compared against generic code simulations. None of the generic code simulations matched the NIF data exactly, however the parameter χ provided the best overall match to the data.

Figure 6.4 in section VI presents the measured NIF data versus the generic code simulations using χ as the ignition parameter. A close inspection of figure 6.4 suggests that the best performing NIF shots are just about to climb up the steepest part of the ignition cliff as seen when using χ as the ignition parameter. Figure 6.4 indicates that a 50% increase in the no-alpha value of χ would most likely be enough to achieve ignition. Such a 50% increase in χ is of the same order of magnitude as the discrepancy between the ICF code's estimate of the hotspot pressure and the actual hotspot pressure inferred directly from the NIF data seen in table 6.4. Hence we are led to the final conclusion that if the origin of the discrepancy in the hotspot pressure could be located and corrected in some way, there is a very good chance that ignition could then be achieved.

Acknowledgements: I would really like to thank Oleg Schilling for suggesting I write a report on ignition parameters. I didn't exactly produce the report Oleg suggested, but he did lead me to see the value of writing down all of this work. I would also like to thank Brian Spears and Baolian Cheng both of whom took the time to explain some of the details of their respective work.

VIII. References

[Lawson 1955] J. D. Lawson, "Some Criteria for a Power producing thermonuclear reactor", (Technical Report). Atomic Energy Research Establishment, Harwell Bershire, U.K.A.E.R.E. GP/R 1807 (December 1955).

[Meldner 1981] Private Communication with Heiner Meldner 1981.

[Slone 1983] Private Communication with Jim Slone 1983.

[Doyas 1984] Private Communication with Richard Doyas 1984.

[Dimonte 1996] Guy Dimonte & Marilyn Schneider, "Turbulent Rayleigh-Taylor instability experiments with variable acceleration", *Phys. Rev. E* **54**, 3740 (1996)

[Larson 1997] Private Communication with Mike Larson 1983.

[Dimonte 2006] Guy Dimonte & Robert Tipton "K-L turbulence model for Rayleigh-Taylor and Richtmyer-Meshkov instabilities" *Journal of Fluids*, **18**, 085101 (2006)

[Betti 2010] Ricardo Betti, et al, "Thermonuclear ignition in inertial confinement fusion and comparison with magnetic fusion", *Plasma of Physics* **17**, 058102 (2010).

[Springer 2011] Paul Springer & Charles Cerjan, "Evaluation of Symcap and THD Performance", LLNL-AR-466575, January 20, 2011.

[Cheng 2014] Baolian Cheng, Thomas J. T. Kwan, Yi-Ming Wang & Steven Batha, "On the thermonuclear ignition criterion at the National Ignition Facility", LA-UR-14-24110, August 5, 2014.

[Lindl 2014] John Lindl, Otto Landen, John Edwards, Ed Moses, "Review of the National Ignition Campaign 2009-2012", *Physics of Plasmas* **21**, 020501 (2014).